HHS Public Access

Author manuscript

Exp Eye Res. Author manuscript; available in PMC 2016 October 01.

Published in final edited form as:

Exp Eye Res. 2015 October ; 139: 22–36. doi:10.1016/j.exer.2015.07.014.

Loss of DJ-1 elicits retinal abnormalities, visual dysfunction, and increased oxidative stress in mice

Vera L. Bonilha[1,2,*], **Brent A. Bell**[2], **Mary E. Rayborn**[2], **Xiaoping Yang**[2], **Charlie Kaul**[2], **Gregory H. Grossman**[2,#a], **Ivy S. Samuels**[2,3], **Joe G. Hollyfield**[1,2], **Chengsong Xie**[4], **Huaibin Cai**[4], and **Karen G. Shadrach**[2]

[1]Department of Ophthalmology, Cleveland Clinic Lerner College of Medicine at Case Western Reserve University, Cleveland, Ohio, United States of America

[2]Department of Ophthalmic Research, Cole Eye Institute, Cleveland Clinic, Cleveland, Ohio, United States of America

[3]Research Service, Louis Stokes Cleveland Veterans Affairs Medical Center, Cleveland, Ohio, United States of America

[4]Laboratory of Neurogenetics, National Institute on Aging, Bethesda, Maryland, United States of America

Abstract

DJ-1/PARK7 mutations or deletions cause autosomal recessive early onset Parkinson's disease (PD). Thus, DJ-1 protein has been extensively studied in brain and neurons. PD patients display visual symptoms; however, the visual symptoms specifically attributed to PD patients carrying DJ-1/PARK7 mutations are not known. In this study, we analyzed the structure and physiology of retinas of 3- and 6-month-old DJ-1 knockout (KO) mice to determine how loss of function of DJ-1 specifically contributes to the phenotypes observed in PD patients. As compared to controls, the DJ-1 KO mice displayed an increase in the amplitude of the scotopic ERG b-wave and cone ERG, while the amplitude of a subset of the dc-ERG components were decreased. The main structural changes in the DJ-1 KO retinas were found in the outer plexiform layer (OPL), photoreceptors and retinal pigment epithelium (RPE), which were observed at 3 months and progressively increased at 6 months. RPE thinning and structural changes within the OPL were observed in the retinas in DJ-1 KO mice. DJ-1 KO retinas also exhibited disorganized outer segments, central decrease in red/green cone opsin staining, decreased labeling of ezrin, broader distribution of ribeye labeling, decreased tyrosine hydroxylase in dopaminergic neurons, and increased 7,8- dihydro-8-oxoguanine-labeled DNA oxidation. Accelerated outer retinal atrophy was observed in DJ-1 KO mice after selective oxidative damage induced by a single tail vein injection of $NaIO_3$, exposing increased susceptibility to oxidative stress. Our data indicate that DJ-1-deficient retinas exhibit signs of morphological abnormalities and physiological dysfunction in association with increased

[*]Corresponding Author: bonilhav@ccf.org.
[#a]Present address: Cleveland Eye Bank, 6700 Euclid Ave. Suite 101, Cleveland, Ohio, United States of America

oxidative stress. Degeneration of RPE cells in association with oxidative stress is a key hallmark of age-related macular degeneration (AMD). Therefore, in addition to detailing the visual defects that occur as a result of the absence of DJ-1, our data is also relevant to AMD pathogenesis.

Keywords

DJ-1 knockout; retina; morphology; physiology; histology; immunohistology; biochemistry; oxidation

1. Introduction

Deletion of or homozygous mutations in the DJ-1 gene (*PARK7* locus) cause early-onset autosomal recessive Parkinson's disease (PD) (Bonifati et al., 2003, Hulleman et al., 2007) but account for only a small portion of all PD cases (Corti et al., 2011). DJ-1, originally identified as a novel oncogene in collaboration with H-ras, has multiple functions involving transcription regulation, cellular transformation, redox-sensitive chaperone activity and anti-oxidative stress. Upon oxidative stress, DJ-1 becomes oxidized, leading to protection against cell death through distinct pathways including scavenging reactive oxygen species (ROS) (Mitsumoto and Nakagawa, 2001, Mitsumoto et al., 2001, Taira et al., 2004, Zhou and Freed, 2005), mitochondrial relocalization, binding to homeodomain interaction protein kinase 1 (HIPK1), functioning as a redox-sensitive molecular chaperone, and interacting with the ubiquitin-proteasome system, among others (Mitsumoto and Nakagawa, 2001, Canet-Aviles et al., 2004, Shendelman et al., 2004, Taira et al., 2004, Takahashi-Niki et al., 2004, Park et al., 2005, Choi et al., 2006, Li et al., 2006, Meulener et al., 2006, Sekito et al., 2006). As such, DJ-1 overexpression protects against oxidative injury, whereas knockdown of DJ-1 increases susceptibility to oxidative injury (Kim et al., 2005, Menzies et al., 2005, Meulener et al., 2005, Park et al., 2005, Yang et al., 2005). These deleterious effects of DJ-1 reductions/loss can be mitigated by restoration of DJ-1 expression (Kim et al., 2005).

We initially reported the identification of DJ-1 peptides in both young and aged retinal pigment epithelium (RPE) lysates using a proteomic approach (Gu et al., 2012). Further studies showed that DJ-1 expression is higher in older eyes, suggesting a correlation between DJ-1 levels of expression and oxidative stress in the retina. More recently, we reported increased levels of DJ-1 and oxidized DJ-1 levels in human RPE lysates from age-related macular degeneration (AMD) donors compared to non-AMD donors (Shadrach et al., 2013). DJ-1 immunoreactivity was observed in the RPE and choriocapillaris from AMD donors with geographic atrophy, and in isolated human Bruch's membrane (BM)/choroid from AMD eyes (Shadrach et al., 2013).

The DJ-1-deficient mice studied here were generated by deleting the first coding exon (exon 2). Examination of the behavior and brain pathology in these mice detected alterations in both motor and dopaminergic function and concluded that DJ-1 deficiency leads to progressive motor deficits without any obvious pathological changes in the nigrostriatal system or spinal motor system and muscles (Chandran et al., 2008). The reported DJ-1/PARK7 mutations include deletions (Bonifati et al., 2003, Ramsey and Giasson, 2010) and missense mutations encoding several DJ-1 variants (Abou-Sleiman et al., 2003);(Hering et

al., 2004); (Ramsey and Giasson, 2010). These mutations are hypothesized to induce a loss of the entire protein or loss-of-function versions of the protein (Bonifati et al., 2003), possibly by interfering with its homodimerization (Tao and Tong, 2003) or by forming unstable higher order complexes (Macedo et al., 2003, Knobbe et al., 2011). Visual symptoms such as dimness, blurring, blunted shapes, double vision and difficulty reading are common features in PD patients (Bodis-Wollner, 2002). However, the visual symptoms specifically attributed to PD patients carrying DJ-1/PARK7 mutations are not known. Therefore, the results presented here are relevant to understand the retinal features in this subset of PD patients. In the present study, we investigated the role of DJ-1 in the retina with a detailed physiological and structural analysis of the retina of these DJ-1 KO mice. Our data indicate that DJ-1-deficient retinas display signs of structural abnormalities and physiological changes in association with increased oxidative stress.

2. Materials and Methods

2.1 DJ-1 knockout (KO) model

Mice with a deletion of the second exon of DJ-1 have been characterized previously (Chandran et al., 2008). Mice were housed in a 12-h light/dark cycle and fed a regular diet ad libitum. All animal procedures were approved by the Institutional Animal Care and Use Committee (IACUC protocol number ARC2013-1048) at the Cleveland Clinic. Homozygous DJ-1 KO mice were backcrossed onto the C57Bl/6J background; our analyses were carried out in both male and female 3- and 6-month-old mice. DJ-1 heterozygous KO mice were not analyzed. For *in vivo* imaging and retinal function experiments, mice were anesthetized with sodium pentobarbital (Nembutal sodium solution, USP, 65 mg/kg), and all efforts were made to minimize procedural stress. Sodium pentobarbital was manufactured by Oak Pharmaceuticals, Inc. (Subsidiary of Akorn, Inc., Lake Forest, IL).

2.2 Genotyping

Genomic DNA was isolated from tail biopsies using DirectPCR Lysis Reagent (mouse tail, Viagen Biotech, Los Angeles, CA) and subjected to PCR amplification using specific sets of PCR primers for the DJ-1 genotype, including mDJ-1-int1-F1 (GGATTAAAGGCATGCAAGGA), mDJ-1Ex2-R (CATCTCCTCTGCTCCTTTG), and Mdj-1-tk-R (GTTATCTGGGCGCTTGTCAT). PCR amplifications were conducted in a total volume of 25 µl, comprising of 1 µl of DNA, 2 µl of primer mixture, and 12.5 µl of Choice Taq master mix (CB4070-8, Denville) and the following conditions: 3 min at 94 °C, followed by 35 cycles of 45 s at 94 °C, 30 s at 58 °C and 90 s at 72 °C and a 5 min extension at 72 °C. PCR products were separated by electrophoresis on a 2% agarose gel and visualized under UV light after staining with Ez-Vision (Amresco). The Crb1 rd8 mutation has been reported to be present in multiple mouse strains. We confirmed the absence of this allele in our mice by PCR amplification as previously described (Mattapallil et al., 2012).

2.3 *In vivo* imaging of retinas

Fundus examination of control and DJ-1 KO mice was made following sodium pentobarbitol anesthesia and pupil dilation with 1.5 µL of 0.5% Mydrin-P drops (Santen Pharmaceutical Co., Ltd., Osaka, Japan) and topical anesthesia 0.5% proparacaine HCl (Bell

et al., 2014). Imaging by scanning laser ophthalmoscopy (SLO) (model HRA2; Heidelberg Engineering, Inc., Vista, CA) and spectral-domain optical coherence tomography (SD-OCT) (model Envisu SDOIS; Bioptigen, Inc., Research Triangle Park, NC) was carried out as previously described (Bell et al., 2012). Infrared (IR) and Autofluorescence (AF) SLO images were obtained using illumination and excitation wavelength of 820 and 488nm, respectively. OCT images (10 individual B-scans) from the horizontal and vertical meridian were collected using 1000 A-scans/B-scan. Images from each meridian were co-registered and averaged using ImageJ and analyzed using Graphpad Prism v6 (see Supplement Fig. S1). Five mice of each genotype and age were analyzed.

2.4 Retinal function

Retinal function of DJ-1 KO and control mice was studied using electroretinogram (ERG) protocols designed to measure function of the outer retina and RPE. All recordings were made after overnight dark adaptation. Mice were anesthetized as described above, their corneas were anesthetized (1% proparacaine HCl), their pupils dilated (1% mydriacyl, 2.5% phenylephrine HCl, 1% cyclopentolate), and the mice were placed on a temperature-regulated heating pad throughout the recording session. ERG components generated by the neural retina were measured in response to strobe flash stimulation using a recording protocol that has been developed for mouse ERG recording as previously described (Samuels et al., 2010). The direct-current coupled (dc)–ERG components generated by the RPE in response to a 7 minute duration stimulus were also recorded and analyzed as previously described (Wu et al., 2004).

2.5 Histology and transmission electron microscopy of retinas

Eyes were enucleated and fixed by immersion in 2% paraformaldehyde, 2.5% glutaraldehyde and 5% $CaCl_2$ made in 0.1 M cacodylate buffer for 30 min at 4°C. Eyecups from both control and DJ-1 KO littermates were post-fixed in 1% osmium tetroxide, dehydrated in a graded series of ethanol to propylene oxide, embedded in epon and polymerized for 48 hrs at 60°C (Bonilha et al., 2006). For bright-field microscopy, semi-thin sections were cut with a diamond histotech knife, collected on glass slides, and stained with toluidine blue. Slides were photographed with a Zeiss AxioImager.Z1 light microscope, and the images were digitized using a Zeiss AxioCam MRc5 camera. For transmission electron microscopy (TEM), the same block of plastic-embedded samples was thin sectioned on an RMC, PowerTome-XL (Tucson, AZ) ultramicrotome, stained with uranyl acetate and lead citrate and viewed in a Tecnai 20–200 kV digital electron microscope (Philips, Hillsboro, OR) equipped with a Gatan image filter and digital camera at 3600 diameters as previously described (Bonilha et al., 2006).

2.5.1 Quantification of the number of vacuoles and RPE thickness—Toluidine blue sections images were acquired 90 μm away from the optic nerve head (on both sides) using identical settings. Images from 4 different mice in each group were acquired and exported to ImageJ 1.43u (http://rsb.info.nih.gog/ij). Images were calibrated from a known reference embedded in the image. The entire height of the RPE cells (from the basal infoldings to the melanin pigments) in six different areas in each image was delineated using the freehand line, measured and a mean thickness was determined for each mouse. Within

this area, the number of vacuoles present in the RPE cytoplasm was manually counted in six different fields of 90 μm in each eye. Samples were analyzed using a two-way repeated-measures ANOVA, with an alpha value of 0.05. The statistical analysis was performed using Graphpad Prism v 6.0a.

2.6 Immunohistochemistry

2.6.1 Cryosections preparation and labeling—After enucleation, eyes were fixed by overnight immersion in 4% paraformaldehyde in PBS at 4°C. Eyes were quenched with 50 mM NH_4Cl for 30 min and then infused successively with 10% and 20% sucrose in PBS, and finally Tissue-Tek "4583" (Miles Inc., Elkhart, IN). Cryosections (8 μm) were cut on a cryostat HM 505E (Microm, Walldorf, Germany) equipped with a CryoJane Tape-Transfer system (Leica Inc., Buffalo Grove, IL). For labeling, sections were washed to remove embedding medium, blocked in PBS supplemented with 1% BSA (PBS/BSA) for 30 min, and incubated with primary followed by secondary antibodies coupled to Alexa 488 and Alexa 594, as well as with TO-PRO-3 for nuclear labeling (Life Technologies, Grand Island, NY) as previously described (Shadrach et al., 2013). A series of 0.5-μm *xy* (*en face*) sections were collected using a laser scanning confocal microscope (Leica TCS-SP8, Exton, PA) using the same acquisition parameters for each channel in the Leica confocal software LAS AF. Antibodies used included PARK7 (TA301239, Origene, Rockville, MD, 1:750), red/green opsin (AB5405, Millipore, Billerica, MA, 1:200), ribeye (CtBP2, 612044, BD Transduction, 1:500), ezrin (MS-661-P0, Thermo Scientific, Rockford, IL, 1:100), tyrosine hydroxylase (TH) (MAB318, Millipore, 1:400), 8-oxoguanine (MAB3560, Millipore, 1:300), and Nrf2 (sc-13032, Santa Cruz Biotechnology, Santa Cruz, CA, 1:100). For DJ-1 staining, sections were processed and labeled as previously described (Gu et al., 2012).

2.6.1 Measurement of ribeye content in the OPL—To quantify ribeye immunoreactivity, images from 4 different mice in each group were acquired using identical settings, exported to ImageJ and calibrated from a known reference embedded in the image. The area of ribeye staining in each image was delineated using the polygon tool to designate regions of interest (ROI), which were subsequently measured. After a threshold was applied to filter out the structures of interest in the ROI, the number of particles was analyzed. Statistical analysis was calculated as described above.

2. 6.2 Whole-mounted retinas preparation and labeling—Enucleated eyes (6 month-old) were fixed for 20 min at 4°C in 4% paraformaldehyde. Retinas were separated from RPE/choroid and stored in blocking buffer (PBS+ 1% BSA+0.1% TX100). Samples were then incubated in anti-red/green opsin antibody in the same blocking buffer overnight at 4°C. Whole-mounted retinas were prepared on glass slides and images were acquired using a laser scanning confocal microscope (Leica TCS SP8) as described above.

2.7 Western Blot Analysis

Mice eyes (6 month-old) were enucleated, the retina/RPE was mechanically detached from the choroid, and lysed by sonication in RIPA buffer (Thermo Scientific) supplemented with a cocktail of protease and phosphatase inhibitors (Sigma). Extracted proteins were quantitated with a Micro BCA protein assay (Thermo Scientific). Lysates (30μg protein)

were loaded into and resolved by SDS-PAGE on 4–20% Novex®-Tris-Glycine gel (Life Technologies) and electro-transferred to Immobilon PVDF membranes (Millipore, Bedford, MA). Membranes were blocked with SuperBlock™ T20 (TBS) Blocking Buffer (Thermo Scientific) for 30 min. and incubated overnight in the same solution with antibodies to PARK7 (DJ-1) (NB300-270, Novus Biologicals, Littleton CO), ezrin (ab41672, Abcam, Cambridge, MA), TH (MAB318, Millipore), Nrf2 (sc-13032, Santa Cruz), red/green opsin (sc-30022, Santa Cruz), GAPDH (ab9484, Abcam). Protein detection was performed with secondary antibodies conjugated to peroxidase and visualized using ECL Plus Western Blotting detection reagent (GE Healthcare Bio-Sciences Corp, Piscataway, NJ). PVDF membranes were exposed to film, films were scanned and figures were composed using Adobe Photoshop CS3. Signal intensities were quantified using ImageJ 1.43u. Mean relative signal intensities were calculated and adjusted to GADH relative intensity from retina/RPE lysates obtained from 3 different mice in each group. Statistical analysis was calculated as described above.

2.8 Sodium iodate-induced degeneration model

Sodium iodate ($NaIO_3$) is an oxidizing agent known to induce selective degeneration and atrophy of RPE cells (Nilsson et al., 1977). Three-month-old DJ-1 KO and control mice (4–7 animals at each time point) received a single tail vein injection of 1% $NaIO_3$ in PBS (25 mg/kg of body weight; Sigma-Aldrich); control animals received PBS. At 1, 3, or 5 days after injection, mice were euthanatized, their eyes were enucleated and processed as described above. Toluidine blue sections images were acquired 90 μm away from the optic nerve head (on both sides) using identical settings, and exported to ImageJ where the mean RPE thickness was measured as described. The number of inflammatory cells infiltrating into the subretinal space was manually counted in six different fields of 90 μm in each eye. Statistical analysis was calculated as described above.

3. Results

3.1 *In vivo* morphological and functional analyses of the retina

In vivo retinal morphology of control and DJ-1 KO mice was analyzed using SLO and SD-OCT (Fig. 1). IR- (images not shown) and AFSLO imaging identified no obvious retinal abnormalities in 3-month- (Fig. 1A) and 6-month-old control (Fig. 1C) and DJ-1 KO mice retinas (Fig. 1B and 1D), respectively. A few autofluorescent foci were visible in 6-month-old control (Fig. 1C, arrowheads), and 3-month- (Fig. 1B, arrowheads) and 6-month-old (Fig. 1D, arrowheads) DJ-1 KO retinas. A collection of cross-sectional, in-depth views using SD-OCT showed intact retinal cell layers in both 3-month- (Fig. 1E) and 6-month-old (Fig. 1G) control retinas. All retinal layers were also visible in both 3-month- (Fig. 1F) and 6-month-old (Fig. 1H) DJ-1 KO retinas. Further review of the DJ-1 KO retinas showed a less well-delineated division between photoreceptor inner and outer segments (yellow brackets). This qualitative image observation was quantified through the analysis of the longitudinal reflectance profile (LRP) of the retina between external limiting membrane and the choriocapillaris to establish layer presence and locate layer boundaries, as previously described (Garcia Garrido et al., 2014). A step-by-step procedure is shown and described in Supplemental Fig. 1. Representative graphs of the mean reflectance signal intensities

normalized to the smallest and largest signal intensities of control mice vs. axial tissue depth are depicted in Fig. 1I and 1J. Six month-old DJ-1 KO mice displayed photoreceptor outer segments that were significantly different from control mice in all eye quadrants (Supplemental Fig. 1F). This observation was specific to the proximal outer segments (nearest to the IS/OS junction and/or inner segments, Fig. 1J, black arrow). At 6-months DJ-1 KO showed evidence of photoreceptor layer thinning in all four quadrants relative to control mice, however, this trend was not significant. A prominent pre-retinal membrane was visible in 100% percent of the DJ-1 KO mice at both 3 and 6 months of age (Fig. 1F and 1H, white arrows). This observation represents a recognizable phenotype for this knockout model. The membrane extends outward from optic disk with conspicuous and increasing separation from the vitreoretinal interface as distance from the optic nerve increases.

We used ERGs to analyze the function of the outer retina and RPE. Average strobe-flash ERG tracings depict both photoreceptor activity in the form of the a-wave and bipolar cell function in the form of the b-wave in response to a range of stimuli at 3 (Fig. 2A) and 6 (Fig. 2B) months of age. Luminance-response functions for the a-wave of the ERG (Fig. 2C) showed no significant difference between control and DJ-1 KO retinas at either age and at all stimuli analyzed. However, the luminance-response functions for the b-wave (Fig. 2D) were significantly increased in the DJ-1 KO retinas compared with controls. On average, the amplitude of the b-wave was increased by 20% in the DJ-1 KO as compared to the WT at 3 ($p<0.004$ for genotype by Two-way ANOVA) and 6 months ($p<0.0001$ for genotype by Two-way ANOVA). The increase in the 3-month-old DJ-1 KO b-wave was significant only at the − 0.6 and 0 log cd s/m^2 stimuli, while in the 6-month-old DJ-1 KO retinas, the b-wave amplitude was significantly increased for the 5 highest luminances tested ($p<0.015$ for each, Two-way ANOVA). The cone ERG in DJ-1 KO retinas was significantly increased by flash luminance, averaging 20% and 30% above wild-type mice at 3 and 6 months of age, respectively (Fig. 2E). For the 3-month-old DJ-1 KO mice, the cone ERG was significantly increased by the 1.4 and 1.9 log cd s/m^2 stimuli ($p<0.01$, Two-way ANOVA), while for the 6-month-old mice, a significant increase occurred in response to 0.4, 0.9, and 1.9 log cd s/m^2 flash stimuli ($p<0.05$ for each by Two-way ANOVA) (Fig. 2F).

Light-evoked responses of the RPE (dc-ERG) were also measured (Fig. 3). Representative dc-ERG tracings, generated secondary to rod photoreceptor activity in the form of a c-wave, fast oscillation, light peak, and off-response measured in 3- and 6-month-old control and DJ-1 KO mice are depicted in Fig. 3A–B. The overall amplitude of the dc-ERG was decreased in the DJ-1 KO mice at both 3 (Fig. 3A) and 6 months (Fig. 3B) of age. However, this effect was only significant for the light peak in 6-month-old mice (a 30% reduction) (Fig. 3D) and the off response of the DJ-1 KO at 3 months of age (50%) (Fig. 3F). All together, these results suggest a tendency of the ERG components generated by the outer retina to increase whereas the ERG components generated by the RPE response diminish in the DJ-1 KO mice.

3. 2 Histological and ultrastructural analysis of the retina

To evaluate the effects of DJ-1 depletion on the structure of the retina, we analyzed immunostained cryosections and toluidine blue-stained cross sections of the retinas from

control and DJ-1 KO mice (Fig. 4). Immunohistological staining of both 3-month- (Fig. 4A) and 6-month-old control mice (Fig. 4C) with DJ-1 antibodies showed that the major distribution of this protein is in RPE and photoreceptor cells, mostly at the inner segments and cell body. Minor distribution of DJ-1 was also observed in the outer plexiform layer (OPL). Qualitative analysis showed that a significant increase in the immunoreactivity of DJ-1 was observed in the 6-month-old RPE and OPL (Fig. 4C). In comparison, the retinas of both 3-month- (Fig. 4B) and 6-month-old (Fig. 4D) DJ-KO mice were completely depleted of DJ-1 reactivity. Cell nuclei labeling of retinas demonstrated that 3-month- (Fig. 4B) and 6-month-old (Fig. 4D) DJ-1 KO mice retinas appeared to be grossly normal when compared to control retinas (Figs. 4A and 4C). However, observation of histological sections from DJ-1 KO mice at high magnification detected morphological changes in the retinal layers that would normally display DJ-1 localization (RPE, photoreceptors and OPL). The OPL contains dendrites of bipolar cells synapsing with axons of photoreceptor cells. Histologically, this region contains several strata of well-defined circular profiles in both the 3-month-old (Fig. 4E) and 6-month-old (Fig. 4I) control retina bodies. In the 3-month-old DJ-1 KO mouse retinas, these circular profiles were less evident (Fig. 4F). The morphological differences in the OPL were also visible by electron microscopy (Fig. 4M, 4N, 4O and 4P). The 3 month-old DJ-1 KO mice displayed several electron lucent structures that appear to be mitochondria in the horizontal cell dendrites (Fig. 4N, black arrows) and in the rod spherules (Fig. 4P, black arrows) when compared to the control OPL (Fig. 4M and 4O, black arrows). In the 6-month-old DJ-1 KO OPL, the cone pedicles were highly visible (Fig. 4J, black arrowheads) in comparison with the control OPL (Fig. 4I). The posterior retina of the DJ-1 KO mice displayed RPE thinning (Fig. 4H and 4L, brackets) when compared to the control RPE (Fig. 4G and 4K, brackets). The mean RPE thickness of the 3-month-old control mice was 4.95 μm but decreased to 4.59 μm in the 3-month-old DJ-1 KO mice; these differences, however, were not statistically significant. In contrast, the differences in mean RPE thickness in 6-month-old control mice (5.80 μm) and DJ-1 KO mice (4.18 μm) were statistically significant (Fig. 4Q). Moreover, 50% of the 3-month-old DJ-1 KO retinas displayed accumulation of vacuoles in the RPE cytoplasm (Fig. 4H, white double arrowheads) when compared to the control RPE (Fig. 4G). The average number of vacuoles present in control RPE cells was 1.8, but in the DJ-1 KO eyes, this number increased to 8.4, which is a statistically significant difference (Fig. 4R). These observations suggest that normal DJ-1 expression is required for the maintenance of retinal architecture.

Ultrastructural analysis of the photoreceptor outer segments and RPE from control and DJ-1 KO mice was also carried out by transmission electron microscopy (Fig. 5). At low magnification, control photoreceptor outer segments displayed the typical flat lobulated discs arranged in parallel stacks (Fig. 5A and C). However, both the 3-month- (Fig. 5B) and 6 month-old (Fig. 5D) DJ-1 KO mice displayed photoreceptor outer segments with osmotic fragility giving the appearance of swollen and disorganized disc membranes (Fig. 5B and D). The RPE apical surfaces of both 3-month- (Fig. 5E) and 6-month-old control mice (Fig. 5G) elaborated apical microvilli (MV), while their basal surface was greatly increased by the presence of basal infoldings (BI). At 3 months, DJ-1 KO mice have extended microvilli with obvious ultrastructural abnormalities (Fig. 5F). These abnormalities were more apparent in 6-month-old DJ-1 KO mice as the apical microvilli collapsed on the apical surface of the

cell (Fig. 5H). An increase in phagolysosomes (PL) was also observed in the RPE cytoplasm in both 3-month- and 6-month-old DJ-1 KO mice (Fig. 5F and 5H). At higher magnification, Bruch's membrane (BM) of both 3-month- (Fig. 5J) and 6-month-old (Fig. 5L) DJ-1 KO mice displayed a thinner inner collagenous layer (ICL) when compared with controls. The distance from the RPE basement membrane (RPEBM) to the ICL and the overall BM thickness were measured and the ICL measurement was divided by the BM measurement to determine the relative ICL thickness. The mean percentage of ICL thickness within the BM of the 3-month-old control mice was 22% (n=5) but decreased to 19% (n=5) in DJ-1 KO mice. Similarly, the mean percentage of ICL thickness within the BM in 6-month-old DJ-1 KO mice was 18% (n=4) in contrast to the 22% found in control mice (n=4). While neither of these changes were statistically significant, they do suggest a decreasing trend in the ICL thickness within the BM structure of the DJ-1 KO mice.

3.3 Immunohistochemical analysis of the retinas

To further analyze cone photoreceptors and the RPE in control and DJ-1 KO mouse retinas, retinas were visualized through labeling with red/green opsin and ezrin antibodies, respectively. Ezrin is an actin-binding protein that localizes to the entire length of the RPE microvilli and basal infoldings (Hofer and Drenckhahn, 1993), (Bonilha et al., 1999), while red/green opsin is confined to the cone outer segments. In control mice, ezrin was distributed along the RPE apical microvilli and basal infoldings in both 3-month (Fig. 6A) and 6-month-old (Fig. 6C) mice. No differences were observed in the labeling of the RPE microvilli and basal infoldings for 3-month-old DJ-1 KO (Fig. 6B) and control (Fig. 6A) retinas. However, 6-month-old DJ-1 KO mice (Fig. 6D) displayed a significant decrease in ezrin labeling relative to controls (Fig. 6C). Observation of the red/green cone opsin labeling suggested reduction in the DJ-1 KO central retinas of both 3-month- (Fig. 6B) and 6-month-old (Fig. 6D) mice when compared to controls. To confirm this observation, whole-mounted retinas of 6 month-old mice were prepared and labeled with the same red/green cone opsin antibody (Figs. 6E and 6F). The whole-mounted retinas of control mice displayed red/green cone opsin homogeneously expressed across the retina (Fig. 6E). However, the DJ-1 KO mice (Fig. 6F) displayed central regions with significantly decreased immunodetection of red/green opsin. These results demonstrate that DJ-1 KO mice have degenerative changes that affect both red/green cone photoreceptors and RPE cells.

Next, we analyzed the impact of DJ-1 absence on the OPL by labeling the mouse retinas with ribeye/CtBP2, a major structural protein of synaptic ribbons (Katsumata et al., 2009). The OPL from both 3-month- (Fig. 7A) and 6-month-old (Fig. 7C) control mice contained a multitude of distinct ribeye-positive ribbons. Both 3-month- (Fig. 7B) and 6-month-old (Fig. 7D, arrowheads) DJ-1 KO mouse retinas had ribeye-positive ribbons expanded through larger areas of the retina than the controls, and the overall intensity of the ribeye labeling was decreased in the retinas of 6-month-old DJ-1 KO mice. Quantification of ribeye-labeled particles (Fig. 7E) and area (Fig. 7F) showed them to be significantly increased in both 3-month and 6-month-old DJ-1 KO mice when compared to control mice. The pathogenesis of PD involves the progressive degeneration of dopaminergic neurons and dopamine (DA) depletion in the nigrostriatal system. Dopaminergic neurons were identified in the neural retina as amacrine and interplexiform cells (Frederick et al., 1982) (Popova, 2014).

Therefore, the distribution of one of the two enzymes involved in DA synthesis, tyrosine hydroxylase (TH), was also analyzed in both control and DJ-1 KO mice. Both 3-month- (Fig. 7G) and 6-month-old (Fig. 7I) control mice displayed TH labeling in the axons of dopaminergic amacrine cells in close association with the inner nuclear layer (arrows). In contrast, both 3-month- (Fig. 7H) and 6-month-old (Fig. 7J) DJ-1 KO mice displayed a noticeable decrease in TH labeling of amacrine cells. The changes in TH staining were more easily observed in three-dimensional projections of the TH labeling (Fig. 7G–J, insets). These results demonstrate that DJ-1 KO mice have degenerative changes that affect their photoreceptor ribbon synapses and decrease TH in amacrine cells.

3.4 Analysis of DJ-1 role in oxidative stress protection the retinas

DJ-1 was reported to stabilize the nuclear factor erythroid 2-related factor 2 (Nrf2) by preventing the interaction of Nrf2 with its inhibitor protein Kelch-like ECH associated protein 1 (keap1) in the cytoplasm (Clements et al., 2006, Malhotra et al., 2008, Gan et al., 2010). Therefore, we examined the Nrf2 distribution in the retinas of control and DJ-1 KO mouse retinas. Nrf2 was observed in the ganglion cell layer, the inner and outer plexiform layers, the photoreceptor inner segments and the RPE in the control mice at both 3 month- (Fig. 8A) and 6 months of age (Fig. 8C). However, Nrf2 immunoreactivity was notably weaker in all of these retinal layers in the DJ-1 KO mice at both 3 (Fig. 8B) and 6 months of age (Fig. 8D). Because Nrf2 is a regulator of oxidative stress response and its presence was decreased in the DJ-1 KO mice, we next analyzed the expression of 7,8- dihydro-8-oxoguanine (8-oxoG), the most abundant oxidized base generated *in vivo* by various types of reactive oxygen species (ROS) in these mice. Low levels of 8-oxoG were observed in the ganglion cell layer, Müller cell processes (Fig. 8E, arrowheads), OPL and the RPE in 3-month-old (Fig. 8E) control mice. In the 6-month-old control retinas, 8-oxoG labeling was prominent in the Müller cell processes extending from the foot-plates (Fig. 8G, arrowheads). In the DJ-1 KO mice, however, 8-oxoG was notably present in more cells in the ganglion cell layer and RPE cells of both 3-month- (Fig. 8F) and 6-month-olds (Fig. 8H) when compared to control mice. In the DJ-1 KO retinas 8-oxoG was also present in the photoreceptor inner segments (Fig. 8F and 8H, arrows). Thus, lack of DJ-1 expression is associated with significant downregulation of Nrf2 and increased oxidation.

3.5 Immunoreactivity of proteins in retina/RPE lysates

The immunohistochemistry data suggested that several of the proteins analyzed displayed decreased signal in DJ-KO mice retinas when compared to control mice. Immunoblots of retina/RPE lysates from 6 month-old mice revealed that DJ-1 KO l retinas displayed significant decreased immunoreactivity of red/green cone opsin, TH, Nrf2, ezrin and DJ-1 when compared to control lysates and normalized to the levels of GAPDH (Fig. 8I). Quantification of these lysates (Fig. 8J) demonstrated a 44% reduction in red/green opsin, a 40% reduction in TH, a 56% reduction in Nrf2 and a 83% reduction in ezrin signal intensity when comparing immunoreactivity in the control lysates.

3.6 Histological analysis of a model RPE degeneration animal model

To test if DJ-1 protects against RPE degeneration *in vivo*, control and DJ-1 KO mice were injected with the oxidizing agent $NaIO_3$ followed by histological analysis of retinal sections 1, 3, and 5 days after injection. This model has previously been shown to induce selective RPE degeneration and atrophy (Nilsson et al., 1977).

One day after injection with $NaIO_3$, DJ-1 KO mice already displayed significant RPE thinning and areas without RPE (Fig. 9F, black arrowhead), while the retinas of control mice displayed normal morphology (Fig. 9B). Three days after $NaIO_3$ injection, DJ-1 KO mice displayed RPE thinning together with the presence of cells located in the subretinal space (Fig. 9G, black arrows), while control mice displayed only RPE thinning (Fig. 9C). Five days after injection with $NaIO_3$, DJ-1 KO mice had complete RPE degeneration together with the presence of immune cells filling extensive areas in the subretinal space (Fig. 9H, white arrows), while the control mice had only a few immune cells in the subretinal space in areas deprived of RPE (Fig. 9D, white arrows). Injection of both control (Fig. 9A) and DJ-1 KO mice with PBS (Fig. 9E) did not lead to visible RPE degeneration. Quantification of RPE thickness demonstrated that the mean RPE thickness of the control and DJ-1 KO mice injected with PBS was 4.67 and 4.52 μm, respectively; these differences were not statistically significant (Fig. 9I). Mice injected with $NaIO_3$ display statistical difference from mice injected with PBS for both control (3.11 μm after 1 day, 2.68 μm after 3 days, and 1.90 μm after 5 days) and DJ-1 KO mice (2.34 μm after one day, 2.48 μm after 3 days, and 1.94 μm after 5 days) (Fig. 9I, brackets). In addition, injected DJ-1 KO mice showed statistically significant decrease in RPE thickness with respect to control mice 1 day after $NaIO_3$ injection (*$p=0.0001$). To further analyze the progression of the $NaIO_3$-induced degeneration, we carried out quantification of the number of inflammatory cells infiltrating into the subretinal space (Fig. 9J). The average number of inflammatory cells infiltrating into the subretinal space in both control and in the DJ-1 KO mice increased with the number of days after injection with $NaIO_3$. However, 3 days after injection with $NaIO_3$, DJ-1 KO mice displayed a significant increase in the number of inflammatory cells infiltrating into their subretinal space with respect to control mice (**$p=0.0076$). Thus, lack of DJ-1 renders the RPE susceptible to increased degeneration at early time points after exposure to $NaIO_3$.

Discussion

PD patients display visual symptoms including dimness, blurring, blunted shapes, double vision and difficulty reading (Bodis-Wollner, 2002). However, visual symptoms specifically associated with DJ-1 mutations and deletions have not been reported. Ours is the first study to characterize DJ-1 function in retinal morphology and physiology through the analysis of DJ-1-deficient mice. We demonstrate here that DJ-1 KO mice develop accelerated progressive retinal abnormalities as they age. A summary of the age-related changes identified is shown in Table 1. Our data indicate that DJ-1-deficient retinas display signs of morphological abnormalities and physiological dysfunction in association with increased oxidative stress. These results emphasize the need for future examination of the eyes of PD patients carrying DJ-1 mutations and deletions.

Although red/green cone opsins were significantly decreased in DJ-1 KO mice, our results showed that the b-wave and cone ERG were significantly increased in these retinas, indicating that lack of DJ-1 leads to removal of inhibitory signaling. Scotopic ERG b-waves reflect light-induced electrical activity in retinal cells post-synaptic to the photoreceptors and are primarily generated by the activity of depolarizing (ON) bipolar cells (Kofuji et al., 2000, Pardue and Peachey, 2014). In addition, the b-wave is also affected by OFF-center bipolar cells and by light-induced activity in amacrine and ganglion cells (Awatramani et al., 2001). Cone ERG responses are generated by ON cone bipolar cells (Sharma et al., 2005). DJ-1 is localized to the OPL that contains the processes and synaptic terminals of photoreceptors, horizontal cells, amacrine and bipolar cells. It is therefore probable that the increase we observed in b-wave and cone ERGs directly results from changes in the structure and/or function of amacrine, horizontal, and bipolar cells due to DJ-1 deficiency. Indeed, our ribeye staining results showed that the DJ-1 KO mice have a significant increase in the number and area covered by the photoreceptor synaptic ribbons. In addition, our immunohistochemical staining and biochemical analysis detected a significant decrease in TH (the limiting enzyme in dopamine production) labeling of amacrine cells. A mouse model in which TH was specifically disrupted in the retina, has been generated and it revealed that retinal dopamine is necessary for high-resolution, light-adapted vision mediated through dopamine D1 and D4 receptors (Jackson et al., 2012). Although retinal dopamine levels were not investigated in this study, the ERG measurements we recorded in the DJ-1 KO mice did not display electrophysiological changes similar to the changes recorded in the TH knockout mice. It has also been reported that use of a selective D1 receptor antagonist (SCH 23390) on the intensity-response function of the frog ERG b- and d-waves in conditions of dark and light adaptation, enhanced the amplitude of the b- and d-waves in both conditions of adaptation (Popova and Kupenova, 2011). Future experiments are needed to determine the specific role of dopamine in the visual defects observed in DJ-1 KO mice.

We have also observed a selective decrease in the light peak of the dc-ERG in the DJ-1 KO mice. The light peak originates from a depolarization of the RPE basolateral membrane and is associated with an increase in its conductance (Gallemore and Steinberg, 1993, Samuels et al., 2010). It is possible that these dc-ERG changes are correlated with the RPE thinning, the ultrastructural disorganization of the RPE basal infoldings (also evident from the decrease in ezrin staining), and with an associated decrease in the expression of channels or transport proteins present in the RPE basal infoldings of the DJ-1 KO mice.

Albeit not significant at 3 months, the SD-OCT LRP analysis of all four retinal regions (superior, inferior, nasal and temporal) showed a trend in photoreceptor thinning in DJ-1 KO mice relative to control mice at 6 months. This change, observed *in vivo*, could be related and attributed to the RPE thinning that was identified by histology. This prominent morphological feature of the retinas from DJ-1 KO mice became statistically significant at 6 months of age. These observations are important because AMD patients with geographic atrophy display areas of complete RPE loss and loss plus thinning (Sarks et al., 1988, Sunness et al., 1999, Zhang et al., 2011). Another prominent feature of the RPE and OPL of the DJ-1 KO mice was the presence of areas of extensive vacuolization suggesting cellular

stress or toxicity, leading likely to cell death (Justilien et al., 2007, El-Sayyad et al., 2011, Omri et al., 2011, Tsai et al., 2011, Mukai et al., 2012).

Our in-vivo SD-OCT analysis detected the presence of pre-retinal membranes in 100% of the DJ-1 KO mice. A pre-retinal membrane is a thin sheet of fibrocellular tissue formed on the inner surface of the retina. It can be caused by changes in the cortical region of the vitreous ‘gel’, where it interacts with the retina. Alternatively, it occurs as a result of a previous eye problem such as a torn or detached retina, trauma, disease, blood vessel abnormality or other condition. In the DJ-1 KO mice, it may form in response to sub-optimal anti-oxidative protection along this interface. Further studies will be needed to understand the cause of pre-retinal membrane in the DJ-1 KO mice.

Our observations showed that the Bruch’s membrane (BM) of the DJ-1 KO mice has a thinner ICL than controls. BM is a pentalaminar structure composed of the RPE basement membrane, inner collagenous layer, middle elastic layer, outer collagenous layer, and the choroidal endothelial cell basement membrane (Hogan and Alvarado, 1967). This extracellular meshwork is a dynamic structure that undergoes modeling of its structure and cellular components during aging and in pathological conditions (Killingsworth et al., 1990, Pauleikhoff et al., 1990, Okubo et al., 1999, Zarbin, 2004, Coffey et al., 2007). Further studies will be needed to understand the correlation between RPE depletion in DJ-1 KO mice and thinning of the BM ICL.

Our data showed that retinas from DJ-1 KO mice retinas displayed a noticeable decrease in amacrine TH cell labeling. Reduced immunoreactivity and innervation of TH-labeled neurons was previously reported in post-mortem eyes of a few PD patients (Nguyen-Legros, 1988). In addition, it was also reported that dopamine concentration is decreased in retinas and the substantia nigra of PD patients (Harnois and Di Paolo, 1990). All together these results suggest that dopaminergic neurons both in the substantia nigra and retina of PD patients display similar features of degeneration.

DJ-1 KO mice retinas displayed significant downregulation of Nrf2 and increased oxidation. The data presented here are in agreement with a previous report demonstrating that Fuchs endothelial corneal dystrophy cells displayed decreased levels of DJ-1 together with impaired Nrf2 nuclear translocation and heightened susceptibility to apoptosis (Bitar et al., 2012). The major cellular antioxidant response is mediated through the antioxidant transcriptional master regulator Nrf2, which regulates the expression of many antioxidant genes (Cho et al., 2006). Under baseline conditions, the cytoplasmic inhibitor protein keap1 binds Nrf2 and sequesters it in the cytoplasm via a ubiquitin-dependent pathway (Itoh et al., 1999, Kobayashi et al., 2004). Upon oxidative stress, Nrf2 translocates to the nucleus and induces constitutive expression of antioxidant genes (Chen and Kunsch, 2004, Sun et al., 2007). Nrf2 levels and activity are also regulated by transcription, degradation, and protein stabilization. DJ-1 stabilizes Nrf2 by preventing its interaction with keap1. DJ-1 also contributes to nuclear translocation of Nrf2, where it heterodimerizes with other transcription regulators (Clements et al., 2006, Malhotra et al., 2008).

The experiments with mice injected with $NaIO_3$, an oxidizing reagent, detected accelerated degeneration of the RPE of DJ-1 KO mice. These results are in agreement with our previous observations that overexpression of full-length DJ-1 in RPE cell cultures prior to exposure to oxidative stress decreased the generation of ROS (Shadrach et al., 2013). DJ-1 is a member of the ThiJ/Pfp1 family of molecular chaperones, which are induced during oxidative stress (Corti et al., 2011). A wide body of literature has demonstrated a protective role for DJ-1 against oxidative stress through distinct pathways in diverse cellular systems (Mitsumoto and Nakagawa, 2001, Canet-Aviles et al., 2004, Taira et al., 2004, Takahashi-Niki et al., 2004, Kim et al., 2005, Park et al., 2005, Choi et al., 2006, Meulener et al., 2006, Junn et al., 2009, Kahle et al., 2009). Overall, our data are in agreement with these previous findings and confirm a role for DJ-1 in the oxidative stress response in the retina by connecting retinal abnormalities and visual dysfunction with increased oxidative stress in DJ-1-deficient mice. The role of DJ-1 in oxidative stress in retinas suggests a possible connection to AMD since oxidative stress-induced physiological dysfunction leading to focal loss of the RPE cells has been implicated as a major factor contributing to geographic atrophy and vision loss in AMD (Beatty et al., 2000, Drobek-Slowik et al., 2007). Therefore, our findings are of relevance to AMD, a disease with defined pathogenesis involving chronic oxidative stress, increased accumulation of lipofuscin in the lysosomes, increased mitochondrial stress, RPE dysfunction, formation of extracellular deposits (drusen), and chronic inflammation in response to many hereditary and environmental risk factors.

Supplementary Material

Refer to Web version on PubMed Central for supplementary material.

Acknowledgments

The authors thank Dr. Neal Peachey for comments on the manuscript. This work is a continuation of studies funded by the NIH grant EY017153 (VLB). This work was also supported by a Department of Veteran's Affairs CDA-2 (ISS), an unrestricted grant from the Research to Prevent Blindness, by the Wolf Family Foundation, and partially supported by the Intramural Research Program of National Institute on Aging (Z01-AG000945) (HC).

Abbreviations

PD	Parkinson's disease
KO	knockout
RPE	retinal pigment epithelium
$NaIO_3$	sodium iodate
ROS	reactive oxygen species
AMD	age-related macular degeneration
BM	Bruch's membrane
TH	tyrosine hydroxylase
8-oxoG	7,8- dihydro-8-oxoguanine

References

Abou-Sleiman PM, Healy DG, Quinn N, Lees AJ, Wood NW. The role of pathogenic DJ-1 mutations in Parkinson's disease. Ann Neurol. 2003; 54:283–286. [PubMed: 12953260]

Awatramani G, Wang J, Slaughter MM. Amacrine and ganglion cell contributions to the electroretinogram in amphibian retina. Vis Neurosci. 2001; 18:147–156. [PubMed: 11347812]

Beatty S, Koh H, Phil M, Henson D, Boulton M. The role of oxidative stress in the pathogenesis of age-related macular degeneration. Surv Ophthalmol. 2000; 45:115–134. [PubMed: 11033038]

Bell BA, Kaul C, Hollyfield JG. A protective eye shield for prevention of media opacities during small animal ocular imaging. Exp Eye Res. 2014; 127:280–287. [PubMed: 25245081]

Bell BA, Kaul C, Rayborn ME, Hollyfield JG. Baseline imaging reveals preexisting retinal abnormalities in mice. Adv Exp Med Biol. 2012; 723:459–469. [PubMed: 22183365]

Bitar MS, Liu C, Ziaei A, Chen Y, Schmedt T, Jurkunas UV. Decline in DJ-1 and decreased nuclear translocation of Nrf2 in Fuchs endothelial corneal dystrophy. Invest Ophthalmol Vis Sci. 2012; 53:5806–5813. [PubMed: 22836768]

Bodis-Wollner I. Visualizing the next steps in Parkinson disease. Arch Neurol. 2002; 59:1233–1234. [PubMed: 12164717]

Bonifati V, Rizzu P, van Baren MJ, Schaap O, Breedveld GJ, Krieger E, Dekker MC, Squitieri F, Ibanez P, Joosse M, van Dongen JW, Vanacore N, van Swieten JC, Brice A, Meco G, van Duijn CM, Oostra BA, Heutink P. Mutations in the DJ-1 gene associated with autosomal recessive early-onset parkinsonism. Science. 2003; 299:256–259. [PubMed: 12446870]

Bonilha VL, Finnemann SC, Rodriguez-Boulan E. Ezrin promotes morphogenesis of apical microvilli and basal infoldings in retinal pigment epithelium. J Cell Biol. 1999; 147:1533–1548. [PubMed: 10613910]

Bonilha VL, Rayborn ME, Saotome I, McClatchey AI, Hollyfield JG. Microvilli defects in retinas of ezrin knockout mice. Exp Eye Res. 2006; 82:720–729. [PubMed: 16289046]

Canet-Aviles RM, Wilson MA, Miller DW, Ahmad R, McLendon C, Bandyopadhyay S, Baptista MJ, Ringe D, Petsko GA, Cookson MR. The Parkinson's disease protein DJ-1 is neuroprotective due to cysteine-sulfinic acid-driven mitochondrial localization. Proc Natl Acad Sci USA. 2004; 101:9103–9108. [PubMed: 15181200]

Chandran JS, Lin X, Zapata A, Hoke A, Shimoji M, Moore SO, Galloway MP, Laird FM, Wong PC, Price DL, Bailey KR, Crawley JN, Shippenberg T, Cai H. Progressive behavioral deficits in DJ-1-deficient mice are associated with normal nigrostriatal function. Neurobiol Dis. 2008; 29:505–514. [PubMed: 18187333]

Chen XL, Kunsch C. Induction of cytoprotective genes through Nrf2/antioxidant response element pathway: a new therapeutic approach for the treatment of inflammatory diseases. Curr Pharm Des. 2004; 10:879–891. [PubMed: 15032691]

Cho HY, Reddy SP, Kleeberger SR. Nrf2 defends the lung from oxidative stress. Antioxid Redox Signal. 2006; 8:76–87. [PubMed: 16487040]

Choi J, Sullards MC, Olzmann JA, Rees HD, Weintraub ST, Bostwick DE, Gearing M, Levey AI, Chin LS, Li L. Oxidative damage of DJ-1 is linked to sporadic Parkinson and Alzheimer diseases. J Biol Chem. 2006; 281:10816–10824. [PubMed: 16517609]

Clements CM, McNally RS, Conti BJ, Mak TW, Ting JP. DJ-1, a cancer- and Parkinson's disease-associated protein, stabilizes the antioxidant transcriptional master regulator Nrf2. Proc Natl Acad Sci USA. 2006; 103:15091–15096. [PubMed: 17015834]

Coffey PJ, Gias C, McDermott CJ, Lundh P, Pickering MC, Sethi C, Bird A, Fitzke FW, Maass A, Chen LL, Holder GE, Luthert PJ, Salt TE, Moss SE, Greenwood J. Complement factor H deficiency in aged mice causes retinal abnormalities and visual dysfunction. Proc Natl Acad Sci USA. 2007; 104:16651–16656. [PubMed: 17921253]

Corti O, Lesage S, Brice A. What genetics tells us about the causes and mechanisms of Parkinson's disease. Physiol Rev. 2011; 91:1161–1218. [PubMed: 22013209]

Drobek-Slowik M, Karczewicz D, Safranow K. The potential role of oxidative stress in the pathogenesis of the age-related macular degeneration (AMD). Postepy Hig Med Dosw. 2007; 61:28–37.

El-Sayyad HI, Sakr SA, Badawy GM, Afify HS. Hazardous effects of fried potato chips on the development of retina in albino rats. Asian Pac J Trop Biomed. 2011; 1:253–260. [PubMed: 23569770]

Frederick JM, Rayborn ME, Laties AM, Lam DM, Hollyfield JG. Dopaminergic neurons in the human retina. J Comp Neurol. 1982; 210:65–79. [PubMed: 6127354]

Gallemore RP, Steinberg RH. Light-evoked modulation of basolateral membrane Cl-conductance in chick retinal pigment epithelium: the light peak and fast oscillation. J Neurophysiol. 1993; 70:1669–1680. [PubMed: 8283222]

Gan L, Johnson DA, Johnson JA. Keap1-Nrf2 activation in the presence and absence of DJ-1. Eur J Neurosci. 2010; 31:967–977. [PubMed: 20377612]

Garcia Garrido M, Beck SC, Muhlfriedel R, Julien S, Schraermeyer U, Seeliger MW. Towards a quantitative OCT image analysis. PloS one. 2014; 9:e100080. [PubMed: 24927180]

Gu X, Neric NJ, Crabb JS, Crabb JW, Bhattacharya SK, Rayborn ME, Hollyfield JG, Bonilha VL. Age-related changes in the retinal pigment epithelium (RPE). PloS one. 2012; 7:e38673. [PubMed: 22701690]

Harnois C, Di Paolo T. Decreased dopamine in the retinas of patients with Parkinson's disease. Invest Ophthalmol Vis Sci. 1990; 31:2473–2475. [PubMed: 2243012]

Hering R, Strauss KM, Tao X, Bauer A, Woitalla D, Mietz EM, Petrovic S, Bauer P, Schaible W, Muller T, Schols L, Klein C, Berg D, Meyer PT, Schulz JB, Wollnik B, Tong L, Kruger R, Riess O. Novel homozygous p.E64D mutation in DJ1 in early onset Parkinson disease (PARK7). Hum Mutat. 2004; 24:321–329. [PubMed: 15365989]

Hofer D, Drenckhahn D. Molecular heterogeneity of the actin filament cytoskeleton associated with microvilli of photoreceptors, Muller's glial cells and pigment epithelial cells of the retina. Histochemistry. 1993; 99:29–35. [PubMed: 8468191]

Hogan MJ, Alvarado J. Studies on the human macula. IV. Aging changes in Bruch's membrane. Arch Ophthalmol. 1967; 77:410–420. [PubMed: 6019564]

Hulleman JD, Mirzaei H, Guigard E, Taylor KL, Ray SS, Kay CM, Regnier FE, Rochet JC. Destabilization of DJ-1 by familial substitution and oxidative modifications: implications for Parkinson's disease. Biochemistry. 2007; 46:5776–5789. [PubMed: 17451229]

Itoh K, Ishii T, Wakabayashi N, Yamamoto M. Regulatory mechanisms of cellular response to oxidative stress. Free Radic Res. 1999; 31:319–324. [PubMed: 10517536]

Jackson CR, Ruan GX, Aseem F, Abey J, Gamble K, Stanwood G, Palmiter RD, Iuvone PM, McMahon DG. Retinal dopamine mediates multiple dimensions of light-adapted vision. J Neurosci. 2012; 32:9359–9368. [PubMed: 22764243]

Junn E, Jang WH, Zhao X, Jeong BS, Mouradian MM. Mitochondrial localization of DJ-1 leads to enhanced neuroprotection. J Neurosci Res. 2009; 87:123–129. [PubMed: 18711745]

Justilien V, Pang JJ, Renganathan K, Zhan X, Crabb JW, Kim SR, Sparrow JR, Hauswirth WW, Lewin AS. SOD2 knockdown mouse model of early AMD. Invest Ophthalmol Vis Sci. 2007; 48:4407–4420. [PubMed: 17898259]

Kahle PJ, Waak J, Gasser T. DJ-1 and prevention of oxidative stress in Parkinson's disease and other age-related disorders. Free Radic Biol Med. 2009; 47:1354–1361. [PubMed: 19686841]

Katsumata O, Ohara N, Tamaki H, Niimura T, Naganuma H, Watanabe M, Sakagami H. IQ-ArfGEF/BRAG1 is associated with synaptic ribbons in the mouse retina. Eur J Neurosci. 2009; 30:1509–1516. [PubMed: 19811534]

Killingsworth MC, Sarks JP, Sarks SH. Macrophages related to Bruch's membrane in age-related macular degeneration. Eye. 1990; 4:613–621. [PubMed: 2226993]

Kim RH, Smith PD, Aleyasin H, Hayley S, Mount MP, Pownall S, Wakeham A, You-Ten AJ, Kalia SK, Horne P, Westaway D, Lozano AM, Anisman H, Park DS, Mak TW. Hypersensitivity of DJ-1-deficient mice to 1-methyl-4-phenyl-1,2,3,6-tetrahydropyrindine (MPTP) and oxidative stress. Proc Natl Acad Sci USA. 2005; 102:5215–5220. [PubMed: 15784737]

Knobbe CB, Revett TJ, Bai Y, Chow V, Jeon AH, Bohm C, Ehsani S, Kislinger T, Mount HT, Mak TW, St George-Hyslop P, Schmitt-Ulms G. Choice of biological source material supersedes oxidative stress in its influence on DJ-1 in vivo interactions with Hsp90. J Proteome Res. 2011; 10:4388–4404. [PubMed: 21819105]

Kobayashi A, Kang MI, Okawa H, Ohtsuji M, Zenke Y, Chiba T, Igarashi K, Yamamoto M. Oxidative stress sensor Keap1 functions as an adaptor for Cul3-based E3 ligase to regulate proteasomal degradation of Nrf2. Mol Cell Biol. 2004; 24:7130–7139. [PubMed: 15282312]

Kofuji P, Ceelen P, Zahs KR, Surbeck LW, Lester HA, Newman EA. Genetic inactivation of an inwardly rectifying potassium channel (Kir4.1 subunit) in mice: phenotypic impact in retina. J Neurosci. 2000; 20:5733–5740. [PubMed: 10908613]

Li HM, Taira T, Maita C, Ariga H, Iguchi-Ariga SM. Protection against nonylphenol-induced cell death by DJ-1 in cultured Japanese medaka (Oryzias latipes) cells. Toxicology. 2006; 228:229–238. [PubMed: 17034925]

Macedo MG, Anar B, Bronner IF, Cannella M, Squitieri F, Bonifati V, Hoogeveen A, Heutink P, Rizzu P. The DJ-1L166P mutant protein associated with early onset Parkinson's disease is unstable and forms higher-order protein complexes. Hum Mol Genet. 2003; 12:2807–2816. [PubMed: 12952867]

Malhotra D, Thimmulappa R, Navas-Acien A, Sandford A, Elliott M, Singh A, Chen L, Zhuang X, Hogg J, Pare P, Tuder RM, Biswal S. Decline in NRF2-regulated antioxidants in chronic obstructive pulmonary disease lungs due to loss of its positive regulator, DJ-1. Am J Respir Crit Care Med. 2008; 178:592–604. [PubMed: 18556627]

Mattapallil MJ, Wawrousek EF, Chan CC, Zhao H, Roychoudhury J, Ferguson TA, Caspi RR. The Rd8 mutation of the Crb1 gene is present in vendor lines of C57BL/6N mice and embryonic stem cells, and confounds ocular induced mutant phenotypes. nvest Ophthalmol Vis Sci. 2012; 53:2921–2927.

Menzies FM, Yenisetti SC, Min KT. Roles of Drosophila DJ-1 in survival of dopaminergic neurons and oxidative stress. Curr Biol. 2005; 15:1578–1582. [PubMed: 16139214]

Meulener M, Whitworth AJ, Armstrong-Gold CE, Rizzu P, Heutink P, Wes PD, Pallanck LJ, Bonini NM. Drosophila DJ-1 mutants are selectively sensitive to environmental toxins associated with Parkinson's disease. Curr Biol. 2005; 15:1572–1577. [PubMed: 16139213]

Meulener MC, Xu K, Thomson L, Ischiropoulos H, Bonini NM. Mutational analysis of DJ-1 in Drosophila implicates functional inactivation by oxidative damage and aging. Proc Natl Acad Sci USA. 2006; 103:12517–12522. [PubMed: 16894167]

Mitsumoto A, Nakagawa Y. DJ-1 is an indicator for endogenous reactive oxygen species elicited by endotoxin. Free Radic Res. 2001; 35:885–893. [PubMed: 11811539]

Mitsumoto A, Nakagawa Y, Takeuchi A, Okawa K, Iwamatsu A, Takanezawa Y. Oxidized forms of peroxiredoxins and DJ-1 on two-dimensional gels increased in response to sublethal levels of paraquat. Free Radic Res. 2001; 35:301–310. [PubMed: 11697128]

Mukai R, Akiyama H, Tajika Y, Shimoda Y, Yorifuji H, Kishi S. Functional and morphologic consequences of light exposure in primate eyes. Invest Ophthalmol Vis Sci. 2012; 53:6035–6044. [PubMed: 22807297]

Nguyen-Legros J. Functional neuroarchitecture of the retina: hypothesis on the dysfunction of retinal dopaminergic circuitry in Parkinson's disease. Surg Radiol Anat. 1988; 10:137–144. [PubMed: 3135618]

Nilsson SE, Knave B, Persson HE. Changes in ultrastructure and function of the sheep pigment epithelium and retina induced by sodium iodate. I. The ultrastructure of the normal pigment epithelium of the sheep. Acta Ophthalmol (Copenh). 1977; 55:994–1006. [PubMed: 579552]

Okubo A, Rosa RH Jr, Bunce CV, Alexander RA, Fan JT, Bird AC, Luthert PJ. The relationships of age changes in retinal pigment epithelium and Bruch's membrane. Invest Ophthalmol Vis Sci. 1999; 40:443–449. [PubMed: 9950604]

Omri S, Behar-Cohen F, de Kozak Y, Sennlaub F, Verissimo LM, Jonet L, Savoldelli M, Omri B, Crisanti P. Microglia/macrophages migrate through retinal epithelium barrier by a transcellular route in diabetic retinopathy: role of PKCzeta in the Goto Kakizaki rat model. Am J Pathol. 2011; 179:942–953. [PubMed: 21712024]

Pardue MT, Peachey NS. Mouse b-wave mutants. Doc Ophthalmol. 2014; 128:77–89. [PubMed: 24395437]

Park J, Kim SY, Cha GH, Lee SB, Kim S, Chung J. Drosophila DJ-1 mutants show oxidative stress-sensitive locomotive dysfunction. Gene. 2005; 361:133–139. [PubMed: 16203113]

Pauleikhoff D, Harper CA, Marshall J, Bird AC. Aging changes in Bruch's membrane. A histochemical and morphologic study. Ophthalmology. 1990; 97:171–178. [PubMed: 1691475]

Popova E. Role of dopamine in distal retina. Journal of comparative physiology A, Neuroethology, sensory, neural, and behavioral physiology. 2014; 200:333–358.

Popova E, Kupenova P. Effects of dopamine D(1) receptor blockade on the intensity-response function of ERG b- and d-waves under different conditions of light adaptation. Vision Res. 2011; 51:1627–1636. [PubMed: 21605587]

Ramsey CP, Giasson BI. L10p and P158DEL DJ-1 mutations cause protein instability, aggregation, and dimerization impairments. J Neurosci Res. 2010; 88:3111–3124. [PubMed: 20806408]

Rasband, WS. ImageJ. U. S. National Institutes of Health; Bethesda, Maryland, USA: 1997–2014. http://imagej.nih.gov/ij/

Samuels IS, Sturgill GM, Grossman GH, Rayborn ME, Hollyfield JG, Peachey NS. Light-evoked responses of the retinal pigment epithelium: changes accompanying photoreceptor loss in the mouse. J Neurophysiol. 2010; 104:391–402. [PubMed: 20484527]

Sarks JP, Sarks SH, Killingsworth MC. Evolution of geographic atrophy of the retinal pigment epithelium. Eye. 1988; 2:552–577. [PubMed: 2476333]

Sekito A, Koide-Yoshida S, Niki T, Taira T, Iguchi-Ariga SM, Ariga H. DJ-1 interacts with HIPK1 and affects H2O2-induced cell death. Free Radic Res. 2006; 40:155–165. [PubMed: 16390825]

Shadrach KG, Rayborn ME, Hollyfield JG, Bonilha VL. DJ-1-dependent regulation of oxidative stress in the retinal pigment epithelium (RPE). PloS one. 2013; 8:e67983. [PubMed: 23844142]

Sharma S, Ball SL, Peachey NS. Pharmacological studies of the mouse cone electroretinogram. Vis Neurosci. 2005; 22:631–636. [PubMed: 16332274]

Shendelman S, Jonason A, Martinat C, Leete T, Abeliovich A. DJ-1 is a redox-dependent molecular chaperone that inhibits alpha-synuclein aggregate formation. PLoS Biol. 2004; 2:e362. [PubMed: 15502874]

Spaide RF, Curcio CA. Anatomical correlates to the bands seen in the outer retina by optical coherence tomography: literature review and model. Retina. 2011; 31:1609–1619. [PubMed: 21844839]

Sun Z, Zhang S, Chan JY, Zhang DD. Keap1 controls postinduction repression of the Nrf2-mediated antioxidant response by escorting nuclear export of Nrf2. Mol Cell Biol. 2007; 27:6334–6349. [PubMed: 17636022]

Sunness JS, Gonzalez-Baron J, Applegate CA, Bressler NM, Tian Y, Hawkins B, Barron Y, Bergman A. Enlargement of atrophy and visual acuity loss in the geographic atrophy form of age-related macular degeneration. Ophthalmology. 1999; 106:1768–1779. [PubMed: 10485549]

Taira T, Saito Y, Niki T, Iguchi-Ariga SM, Takahashi K, Ariga H. DJ-1 has a role in antioxidative stress to prevent cell death. EMBO Rep. 2004; 5:213–218. [PubMed: 14749723]

Takahashi-Niki K, Niki T, Taira T, Iguchi-Ariga SM, Ariga H. Reduced anti-oxidative stress activities of DJ-1 mutants found in Parkinson's disease patients. Biochem Biophys Res Commun. 2004; 320:389–397. [PubMed: 15219840]

Tao X, Tong L. Crystal structure of human DJ-1, a protein associated with early onset Parkinson's disease. J Biol Chem. 2003; 278:31372–31379. [PubMed: 12761214]

Thevenaz P, Ruttimann UE, Unser M. A pyramid approach to subpixel registration based on intensity. IEEE Trans Image Process. 1998; 7:27–41. [PubMed: 18267377]

Tsai RK, He MS, Chen ZY, Wu WC, Wu WS. PKCdelta-dependent signaling mediates ethambutol-induced toxic effects on human retinal pigment cells. Mol Vis. 2011; 17:1564–1576. [PubMed: 21738386]

Wu J, Peachey NS, Marmorstein AD. Light-evoked responses of the mouse retinal pigment epithelium. J Neurophysiol. 2004; 91:1134–1142. [PubMed: 14614107]

Yang Y, Gehrke S, Haque ME, Imai Y, Kosek J, Yang L, Beal MF, Nishimura I, Wakamatsu K, Ito S, Takahashi R, Lu B. Inactivation of Drosophila DJ-1 leads to impairments of oxidative stress response and phosphatidylinositol 3-kinase/Akt signaling. Proc Natl Acad Sci U S A. 2005; 102:13670–13675. [PubMed: 16155123]

Zarbin MA. Current concepts in the pathogenesis of age-related macular degeneration. Arch Ophthalmol. 2004; 122:598–614. [PubMed: 15078679]

Zhang K, Hopkins JJ, Heier JS, Birch DG, Halperin LS, Albini TA, Brown DM, Jaffe GJ, Tao W, Williams GA. Ciliary neurotrophic factor delivered by encapsulated cell intraocular implants for treatment of geographic atrophy in age-related macular degeneration. Proc Natl Acad Sci U S A. 2011; 108:6241–6245. [PubMed: 21444807]

Zhou W, Freed CR. DJ-1 up-regulates glutathione synthesis during oxidative stress and inhibits A53T alpha-synuclein toxicity. J Biol Chem. 2005; 280:43150–43158. [PubMed: 16227205]

Highlights

- First report of the visual defects due to the absence of DJ-1 expression in mice retinas
- DJ-1 KO mice displayed an increase in the amplitude of b-wave and cone ERGs, while the amplitude of the dc-ERG components were decreased
- DJ-1 KO retinas displayed main structural changes in the outer plexiform layer, photoreceptors and retinal pigment epithelium
- DJ-1-deficient retinas changes are associated with increased oxidative stress

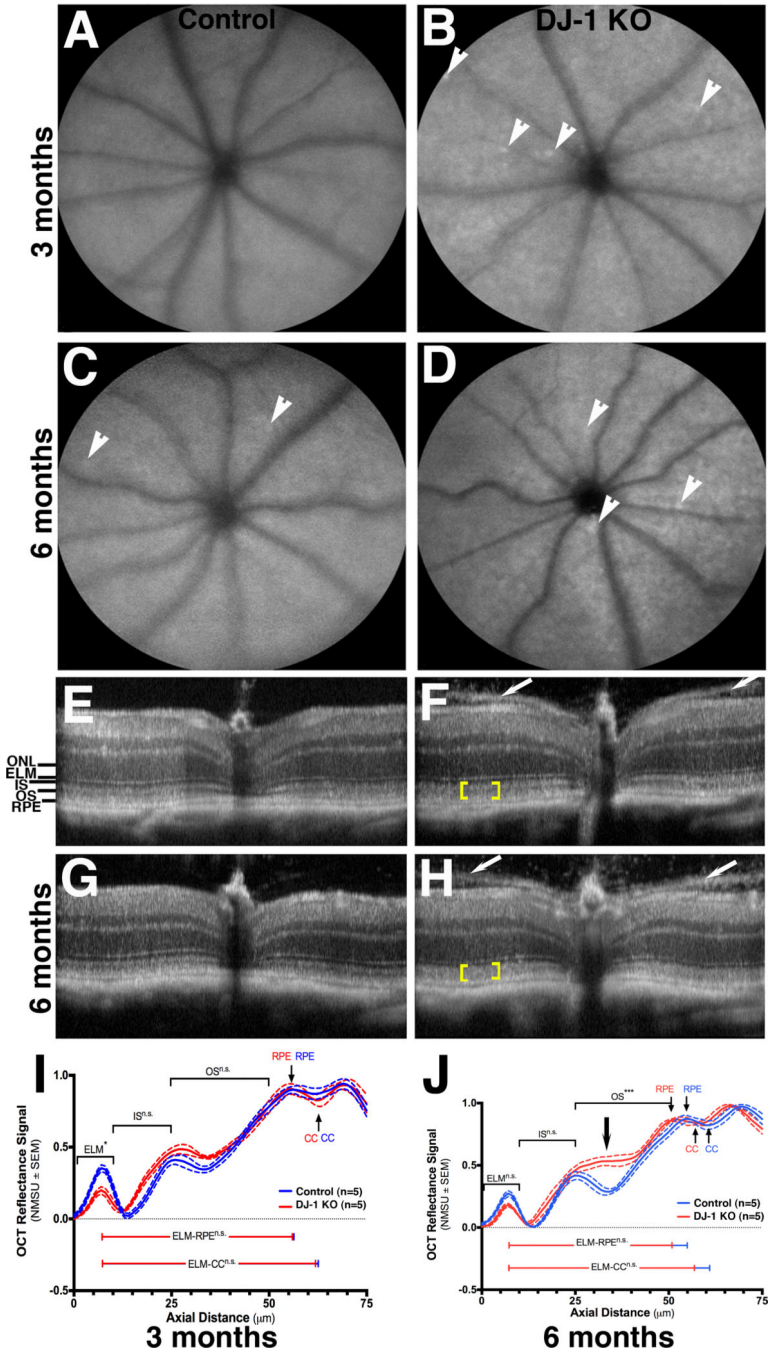

Fig. 1. Mild morphological changes in the retinas of DJ-1 KO mice through *in vivo* structural analysis

A–D: Representative scanning laser ophthalmoscopy (SLO) autofluorescence of the retina of 3-month- (A) and 6-month-old (C) control mice compared to 3-month- (B) and 6-month-old (D) DJ-1 KO mice. White arrowheads show the presence of autofluorescent foci. E–H: Spectral-domain optical coherence tomography (SD-OCT) of the retina of 3 month- (E) and 6 month-old (G) control mice compared to 3-month- (F) and 6-month-old (H) DJ-1 KO mice. Yellow brackets indicate loss of laminar delineation between photoreceptor inner (IS)

and outer segments (OS); white arrows indicate the pre-retinal membrane seen on both sides of the optic nerve. I–J: Analysis of a representative normalized OCT mean reflectance signal of photoreceptor (nasal quadrant) vs. axial tissue depth in 3-month- (I) and 6-month-old (J) mice. The photoreceptor signal was subdivided as follows: ELM= external limiting membrane; IS= inner segments; OS= outer segments; RPE= retinal pigment epithelium; CC= choriocapillaris; ONL= outer nuclei layer. Blue line = control mice, red lines = DJ-1 KO mice. P-values= 3 m.o. ELM (0.0197); 6 m.o. ELM (ns); 3 m.o. OS (n.s.); 6 m.o. OS (0.0004). **J:** black arrow denotes the region of relative change in PL signal, which corresponds to the proximal OS region that is immediately adjacent to the IS/OS junction.

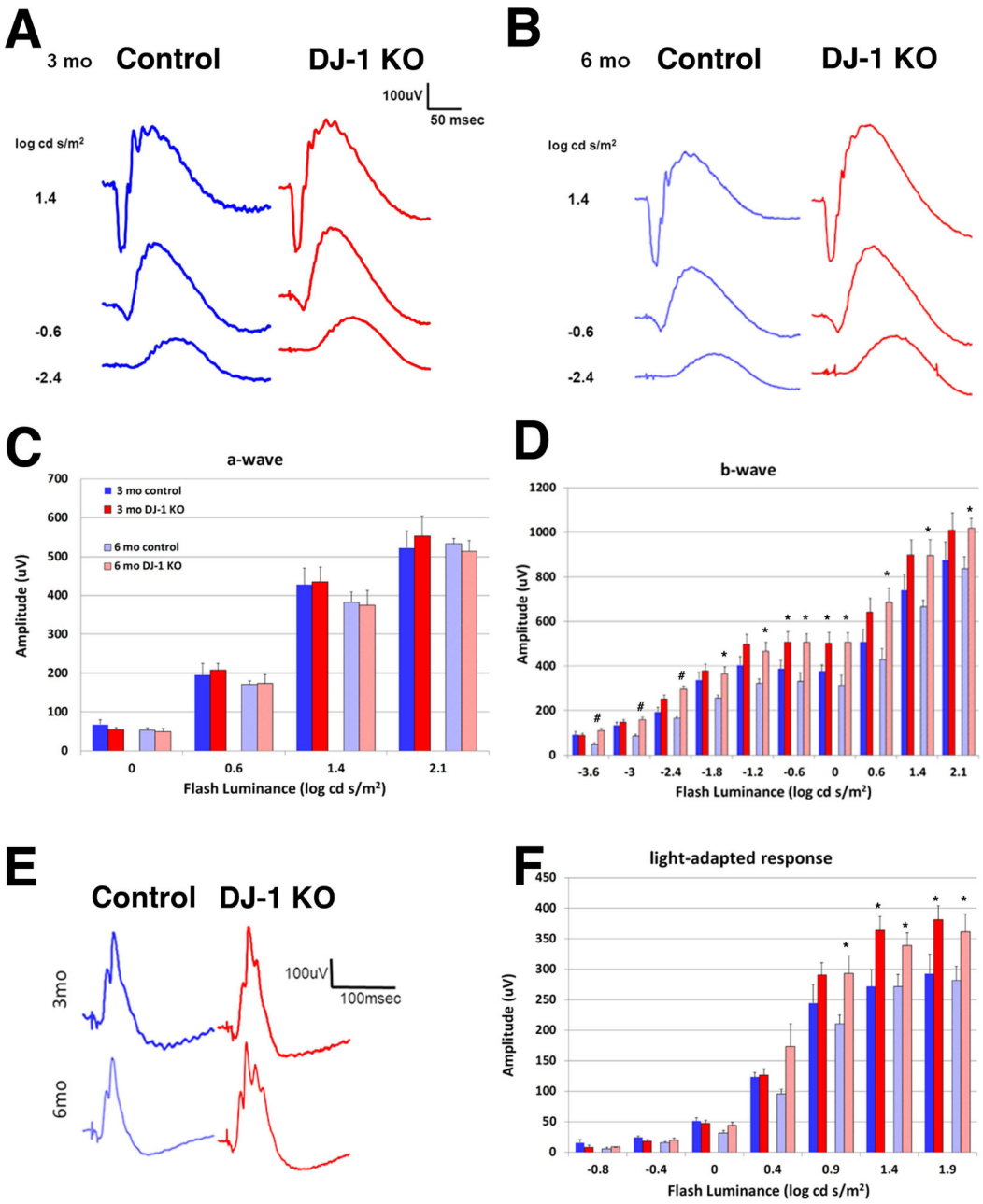

Fig. 2. Increase in scotopic ERG b-wave and in cone ERG amplitudes of DJ-1 KO mice

Averaged strobe-flash ERG tracings were measured at 3-month- (A) and 6-month-old (B) mice. Dark blue tracing depicts response from 3-month-old control mice, light blue tracing depicts response from 6-month-old control mice, dark red tracing depicts response from 3-month-old DJ-1 KO mice, and light red tracing is the response from 6-month-old DJ-1 KO mice. Plotted ERG a-wave (C) and b-wave (D) amplitudes from control and DJ-1 KO mice in both ages at all of the stimuli analyzed. Representative (E) and plotted (F) light-adapted responses; $p<0.004$ for the b-wave of 3 month-old DJ-1 KO mice and $p<0.0001$ for 6 month-old DJ-1 KO mice, $p<0.01$ for the cone ERG of 3-month-old DJ-1 KO mice in

response to 1.4 and 1.9 log cd s/m^2 stimuli, $p<0.05$ for the cone ERG of 6-month-old mice in response to 0.4, 0.9, and 1.9 log cd s/m^2 flash stimuli. Dark blue columns = control 3 month-old mice, dark red columns = DJ-1 KO 3 month-old mice; light blue columns = control 6 month-old mice, light red columns = DJ-1 KO 6 month-old mice.

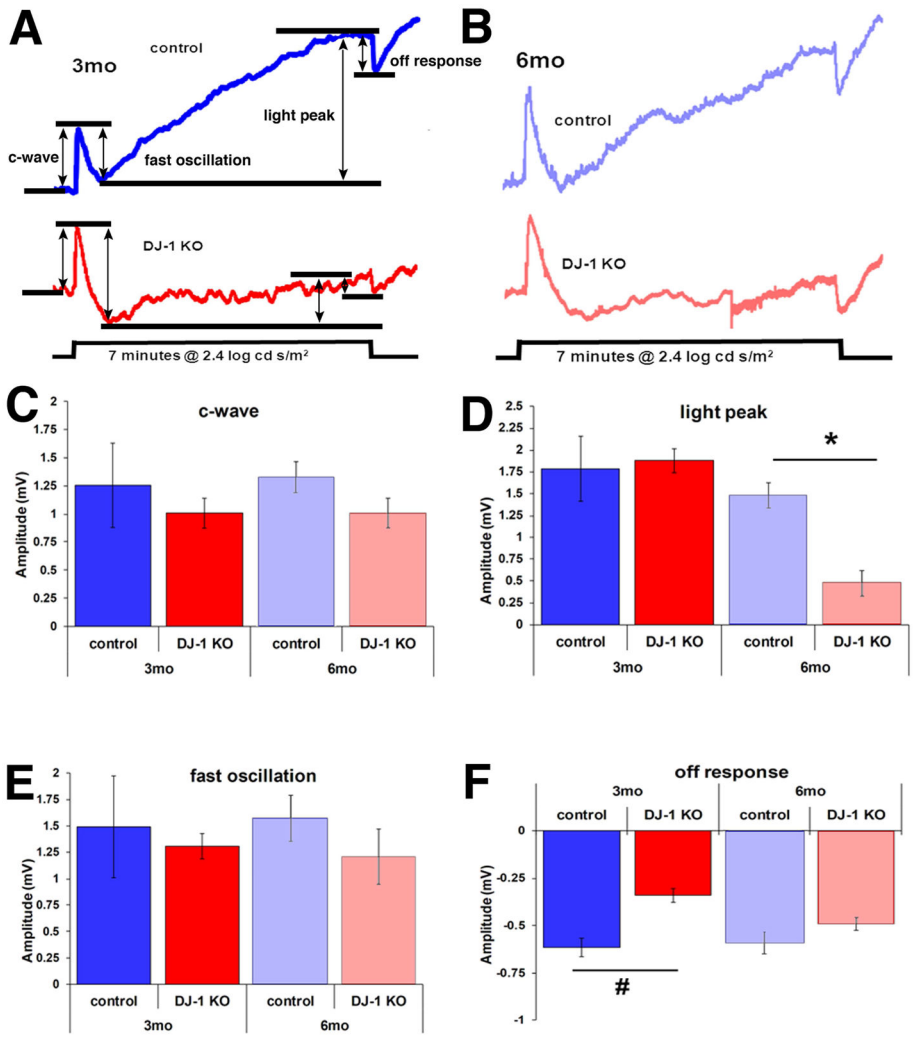

Fig. 3. Decrease in dc-ERG in the retinas of DJ-1 KO mice

dc-ERG tracings were measured at 3 (A) and 6 (B) months. Dark blue tracing depicts a representative response from 3-month-old control mice, light blue tracing depicts response from 6-month-old control mice, dark red tracing depicts response from 3-month-old DJ-1 KO mice, and light red tracing is the response from 6-month-old DJ-1 KO mice. Plotted ERG c-wave (C), light peak (D), fast oscillation (E) and off-response (F) signals in both control and DJ-1 KO retinas in both ages, *p=0.0039; #p=0.0120. Dark blue columns = control 3 month-old mice, dark red columns = DJ-1 KO 3 month-old mice; light blue columns = control 6 month-old mice, light red columns = DJ-1 KO 6 month-old mice.

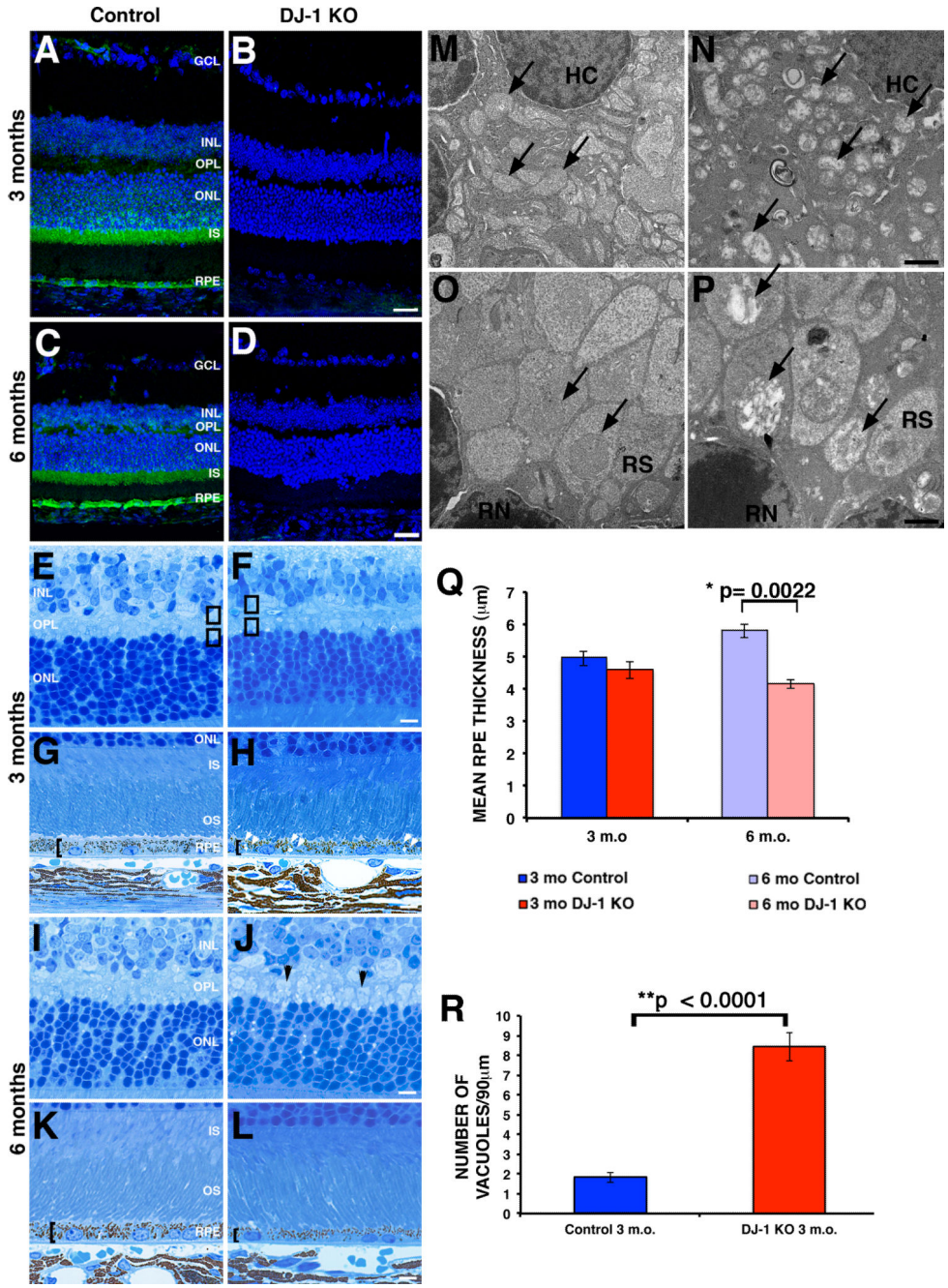

Fig. 4. Morphological abnormalities in the retinas of DJ-1 KO mice

A–D: Confocal microcopy analysis of double immunofluorescent staining of DJ-1 (green) and nuclei (blue) in retina sections from 3- (A) and 6-month-old (C) control, and 3- (B) and 6-month-old (D) DJ-1 KO mice. E–L: Toluidine blue staining of 1 μm plastic sections of retinas from 3-month- (**E, G**) and 6-month-old (**I,** K) control mice compared to 3-month- (F, H) and 6-month-old (**J, L**) DJ-1 KO mice analyzed by bright-field microscopy. **M, N, O, P**: Representative electron micrographs of the OPL of 3-month-old control (M, O) and DJ-1 KO **(N, P)** retinas. **Q**: Plotted data representing the mean RPE thickness ± SEM (n=4). Dark blue columns = control 3 month-old mice, dark red columns = DJ-1 KO 3 month-old mice;

light blue columns = control 6 month-old mice, light red columns = DJ-1 KO 6 month-old mice. Asterisks denote statistical significance with respect to control mice (*p=0.0022). **R**: Plotted data representing the mean number of cytoplasmic vacuoles in the RPE ± SEM (n=3). Asterisks denote statistical significance with respect to control mice calculated by a two-way repeated-measures ANOVA with an alpha of 0.05 (**p<0.0001). Black brackets show RPE thinning; black arrowheads show cone pedicles within the OPL; white double arrowheads show accumulation of vacuoles within the RPE cytoplasm; black arrows show mitochondria in the OPL; black boxes represent areas in the OPL analyzed by electron microscopy. OS, photoreceptor outer segments; IS, photoreceptor inner segments; ONL, outer nuclear layer; OPL, outer plexiform layer; INL, inner nuclear layer; GCL, ganglion cell layer, HC, horizontal cell, RS, rod spherules, RN, rod nuclei. Scale bars A–D: 40μm; E–L: 5 μm; M, N, O, P: 1 μm.

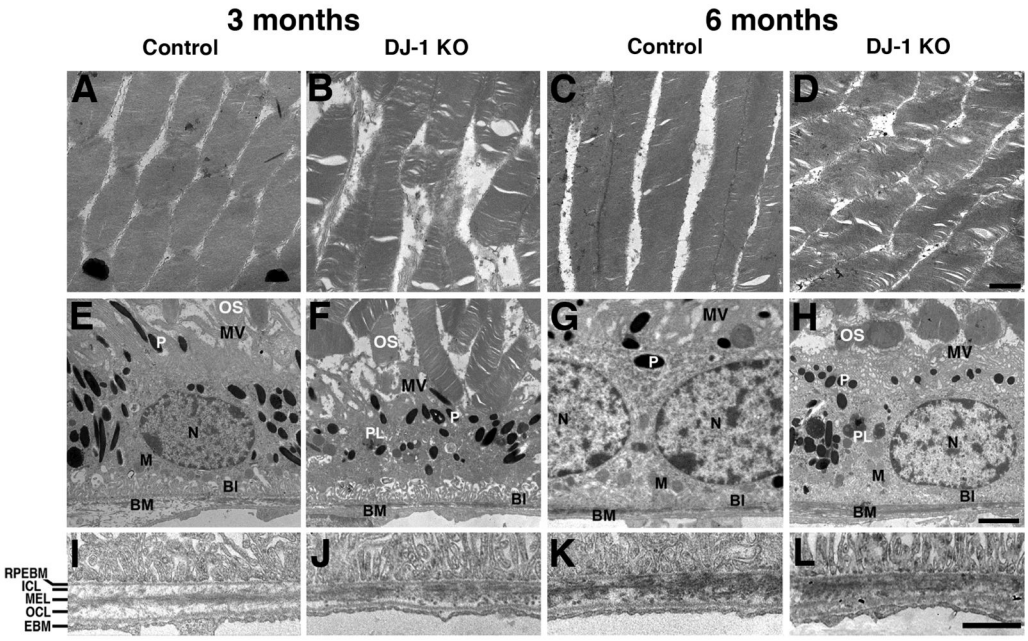

Fig. 5. Ultrastructural abnormalities in the retinas of DJ-1 KO mice

Representative electron micrographs of the photoreceptor outer segments from 3-month- (A) and 6-month-old (C) control, and 3-month- (B) and 6-month-old (D) DJ-1 KO mice. Representative electron micrographs of RPE from 3-month- (E) and 6-month-old (G) control, and 3-month- (F) and 6-month-old (H) DJ-1 KO mice. I–L: High magnification of retinas of 3-month- (E) and 6-month-old (G) control mice compared to 3-month- (F) and 6-month-old (H) DJ-1 KO mice. P, pigment granules; BI, basal infoldings; BM, Bruch's membrane; N, nuclei; PL, phagolysosomes; M, mitochondria; RPEBM, RPE basement membrane; ICL, inner collagenous layer; MEL, middle elastic layer; OCL, outer collagenous layer; EBM, choroidal cell basement membrane. Scale bars A–D: 1 μm; E–H: 2 μm; I–L: 1 μm.

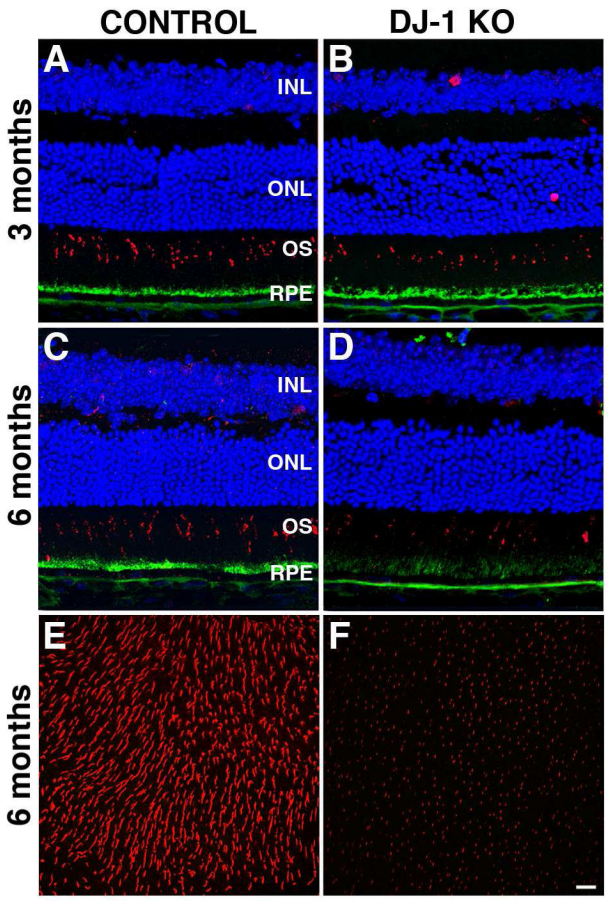

Fig. 6. Abnormalities in RPE and red/green cones in the retinas of DJ-1 KO mice

Representative confocal microscopy images of immunofluorescent staining of cryosections (A–D) and whole-mount (E–F) retinas. Retina sections were labeled with ezrin (RPE marker, green), red/green cone opsin (red), and nuclei (blue) from 3-month- (A) and 6-month-old (C) control, and 3-month- (B) and 6-month-old (D) DJ-1 KO mice. Whole-mounted retinas of 6 month-old control (E) and DJ-1 KO (F) mice were also labeled with red/green cone opsin antibodies. INL, inner nuclear layer; ONL, outer nuclear layer; OS, photoreceptor outer segments. Scale bars: 20 μm.

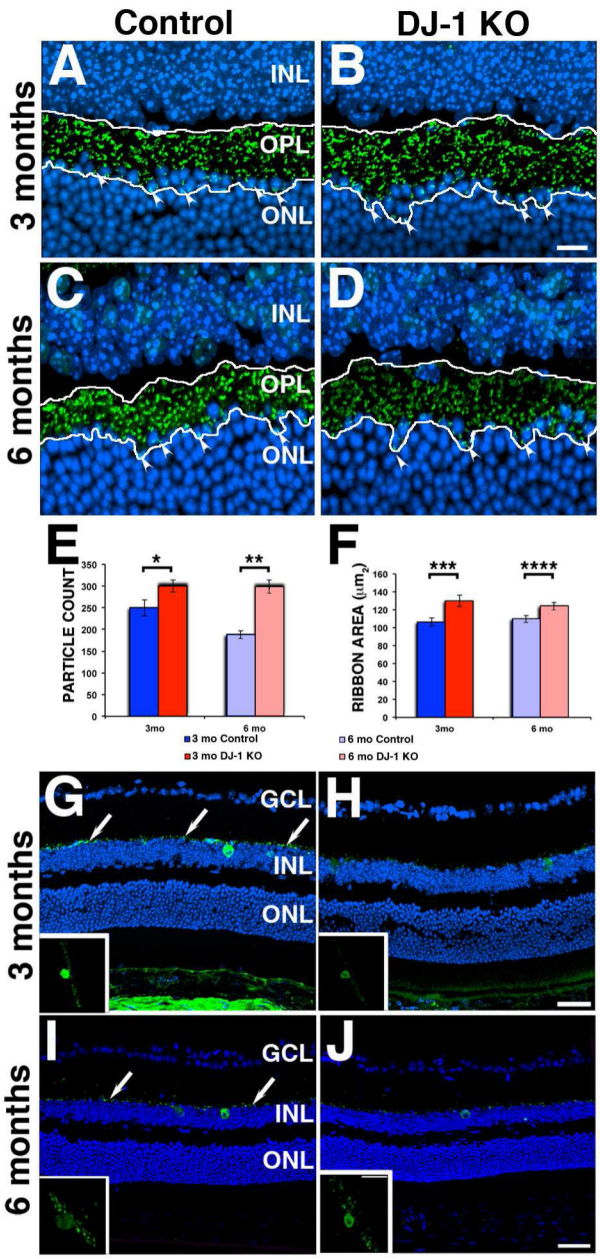

Fig. 7. Photoreceptor synaptic terminals and dopaminergic neurons abnormalities in the retinas of DJ-1 KO mice

Representative confocal microscopy images of immunofluorescent staining of ribeye (synaptic ribbon marker, green) and nuclei (blue) in retina sections from 3-month- (A) and 6-month-old (C) control, and 3-month- (B) and 6-month-old (D) DJ-1 KO mice. White arrowheads show ribeye staining in the ONL of the DJ-1 KO mice; white tracing delineates the area of ribeye staining. E: count of ribeye-stained particles in retinas from the samples described above. F: area covered by the ribeye-stained particles in DJ-1 KO mice, dark and light red bars; 3- and 6 month-old control mice, dark and light blue bars, respectively. Data are expressed as the mean ± SEM; n = 4 eyes per group (A–D). p-values obtained using a t-

test, *p = 0.0431, ** p = 0.0036, ***p = 0.0145, ****p = 0.0384. G–J: Representative confocal microscopy images of immunofluorescent staining of tyrosine hydroxylase (TH, dopaminergic neurons marker, green) and nuclei (blue) in retina sections from 3-month- (G) and 6-month-old (I) control, and 3-month- (H) and 6-month-old (J) DJ-1 KO mice. Insets represent TH staining in a 35°-view angle. White arrows show axonal TH labeling. INL, inner nuclear layer; OPL, outer plexiform layer; ONL, outer nuclear layer. Scale bars A–D: 10 μm; G–J: 40 μm; insets: 10 μm.

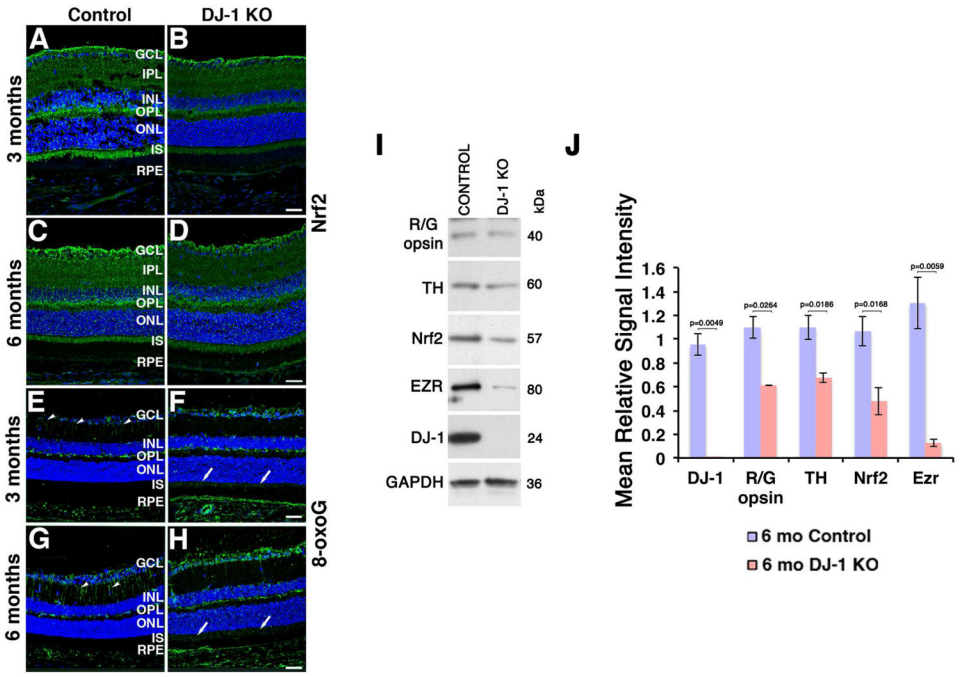

Fig. 8. Increased oxidative stress and inflammation in the retinas of DJ-1 KO mice

A–D: Representative confocal microscopy images of immunofluorescent staining of Nrf2 (oxidative stress regulator, green), and nuclei (blue) in retina sections from 3-month- (A) and 6-month-old (C) control, and 3-month- (B) and 6-month-old (D) DJ-1 KO mice. E–H: Representative confocal microscopy images of immunofluorescent staining for 8-oxoG (DNA oxidation marker, green), and nuclei (blue) in retina sections from 3-month- (E) and 6-month-old (G) control, and 3-month- (F) and 6-month-old (H) DJ-1 KO analyzed by confocal microscopy. I: Representative immunoblots of 6 month-old retina/RPE lysates from control and DJ-1 KO mice reacted with antibodies to red/green opsin (R/G), TH, Nrf2, ezrin (EZR) and DJ-1. J: Quantification of immunoblots of retina/RPE lysates from control (light blue columns) and DJ-1 KO mice (light red columns). Data expressed as mean relative signal intensity ± SEM (n=3), p-values obtained using a t-test. GCL, ganglion cell layer; IPL, inner plexiform layer; INL, inner nuclear layer; OPL, outer plexiform layer; ONL, outer nuclear layer; IS, photoreceptor inner segments; R/G opsin, red/green cone opsin; TH, tyrosine hydroxylase. Scale bars: 40 μm.

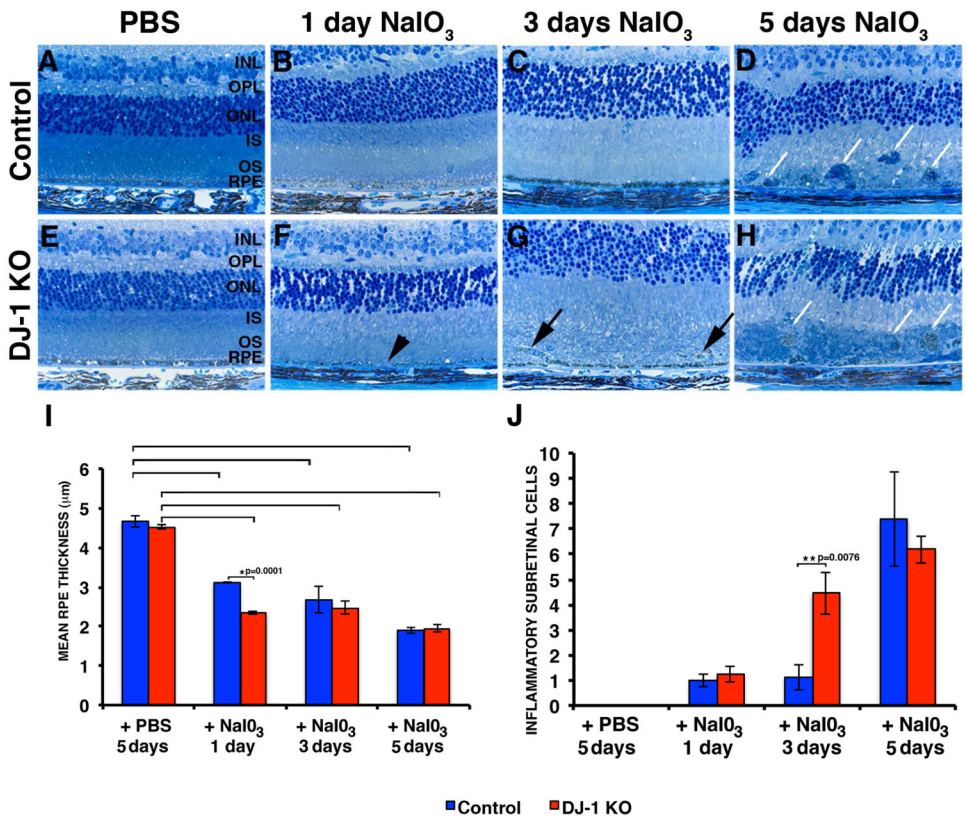

Fig. 9. Accelerated retinal atrophy after a single tail vein injection of $NaIO_3$ in DJ-1 KO mice

Representative images of toluidine blue staining of 1 µm plastic sections of retinas of both control (E–H) and DJ-1 KO (A–D) mouse retinas shown at 1 (B, F), 3 (C, G), and 5 (D, H) days after injection. Both DJ-1 KO (E) and control (A) mice were also injected with PBS. Black arrowhead indicates area without RPE; black arrows show the presence of cells located in the subretinal space; white arrows indicate immune cells filling extensive areas in the subretinal space. INL, inner nuclear layer; OPL, outer plexiform layer; ONL, outer nuclear layer; IS, photoreceptor inner segments. Scale bars: 10 µm. I: Plotted data representing the mean RPE thickness ± SEM (n=7). Red columns = DJ-1 KO; blue columns = control mice. Asterisks denote statistical significance with respect to control mice (*p=0.0001); brackets denote that mice injected with $NaIO_3$ display statistical difference from mice injected with PBS for both control (p= 0.0001 in mice injected with $NaIO_3$ for 1 day, p=0.0201 in mice injected with $NaIO_3$ for 3 days and p= 0.0001 in mice injected with $NaIO_3$ for 5 days) and DJ-1 KO (p= 0.0001 in mice injected with $NaIO_3$ for 1 day, p=0.0004 in mice injected with $NaIO_3$ for 3 days and p= 0.0001 in mice injected with $NaIO_3$ for 5 days) mice. J: Plotted data depicting the mean number of inflammatory cells in the subretinal space ± SEM (n=7). Asterisks denote statistical significance with respect to control mice (**p=0.0076).

Table 1

Summary of age-related retinal changes identified in control and DJ-1 KO mice.

Methodology	3 m.o. Control	3 m.o. DJ-1 KO	6 m.o. Control	6 m.o. DJ-1 KO
IR-SLO	no abnormalities	no abnormalities	no abnormalities	no abnormalities
AF-SLO	no abnormalities	no abnormalities, presence of a few autofluorescent foci	no abnormalities, presence of a few autofluorescent foci	no abnormalities, presence of a few autofluorescent foci
SD-OCT	no abnormalities	no abnormalities, pre-retinal membrane	no abnormalities	no abnormalities, POS significantly different, pre-retinal membrane
a-wave ERG	present	present	present	present
b-wave ERG	present	20% increase	present	20% increase
cone ERG	present	20% increase	present	30% increase
dc-ERG	present	50% decrease (off response)	present	30% decrease (light peak)
TEM	normal	presence of electron lucent structures in OPL (horizontal cell dendrites and rod spherules), POS and MV disorganization, thinner BM ICL	normal	POS and MV disorganization, thinner BM ICL
Histology	normal	RPE thinning not statistically significant	normal	RPE thinning statistically significant (*)
EZR distribution	localized to apical MV and BI	localized to apical MV and BI	localized to apical MV and BI	decreased presence in apical MV and BI
R/G opsin	staining localized to cone outer segments	decreased presence in cone outer segments	staining localized to cone outer segments	decreased presence in cone outer segments
ribeye staining	localized to synaptic ribbons in the OPL	statistically significant (*)increase in ribeye-labeled particles and area	localized to synaptic ribbons in the OPL	statistically significant (*)increase in ribeye-labeled particles and area
TH staining	present in axons of dopaminergic amacrine cells	decreased presence in axons of dopaminergic amacrine cells	present in axons of dopaminergic amacrine cells	decreased presence in axons of dopaminergic amacrine cells
Nrf2 staining	present in GCL, IPL, OPL, IS, RPE	decreased presence in GCL, IPL, OPL, IS, RPE	present in GCL, IPL, OPL, IS, RPE	decreased presence in GCL, IPL, OPL, IS, RPE
8-oxoG staining	low levels in GCL, Müller cell processes, OPL, RPE	prominent in GCL, OPL, IS, RPE	prominent in Müller cell processes, OPL	prominent in GCL, OPL, IS, RPE
retina/RPE lysates immunoreactivity	not evaluated	not evaluated	normal	statistically significant (*)decrease in R/G opsin, TH, Nrf2, EZR and DJ-1 signals

AF-SLO, autofluorescence-scanning laser ophthalmoscopy; SD-OCT, spectral-domain optical coherence tomography; POS, photoreceptor outer segments; TEM, transmission electron microscopy; MV, microvilli; BM ICL, Bruch's membrane inner collagenous layer; EZR, ezrin; BI, basal infoldings; R/G opsin, red/green opsin; OPL, outer plexiform layer; TH, tyrosine hydroxylase; GCL, ganglion cell layer; IPL, inner plexiform layer; IS, photoreceptor inner segments; RPE, retinal pigment epithelium; 8-oxoG, 7,8- dihydro-8-oxoguanine.